Entraining gravity currents

Christopher G. Johnson† and Andrew J. Hogg

Department of Mathematics, University of Bristol, Bristol BS8 1TW, UK

Entrainment of ambient fluid into a gravity current, while often negligible in laboratory-scale flows, may become increasingly significant in large-scale natural flows. We present a theoretical study of the effect of this entrainment by augmenting a shallow water model for gravity currents under a deep ambient with a simple empirical model for entrainment, based on experimental measurements of the fluid entrainment rate as a function of the bulk Richardson number. By analysing long-time similarity solutions of the model, we find that the decrease in entrainment coefficient at large Richardson number, due to the suppression of turbulent mixing by stable stratification, qualitatively affects the structure and growth rate of the solutions, compared to currents in which the entrainment is taken to be constant or negligible. In particular, mixing is most significant close to the front of the currents, leading to flows that are more dilute, deeper and slower than their non-entraining counterparts. The long-time solution of an inviscid entraining gravity current generated by a lock-release of dense fluid is a similarity solution of the second kind, in which the current grows as a power of time that is dependent on the form of the entrainment law. With an entrainment law that fits the experimental measurements well, the length of currents in this entraining inviscid regime grows with time approximately as $t^{0.447}$. For currents instigated by a constant buoyancy flux, a different solution structure exists in which the current length grows as $t^{4/5}$. In both cases, entrainment is most significant close to the current front.

Key words: gravity currents, mixing and dispersion, shallow water flows

---

1. Introduction

Gravity currents – the predominantly horizontal spreading of a dense fluid in a relatively buoyant ambient due to gravity – occur frequently and at very large scales in the atmosphere and oceans. They may be entirely natural phenomena, such as sea-breeze fronts, estuarine currents or pyroclastic flows, or they may occur due to human activity, such as when a dense or buoyant industrial effluent is pumped into a river or ocean (Simpson 1999). While high Reynolds number gravity currents are a fundamental component of environmental flows, their turbulent nature means that the modelling and understanding of these currents remains an active topic of research.

The extent to which a gravity current is diluted, through mixing of the current with surrounding ambient fluid, is of particular interest in currents generated by the release of industrial effluents or pollutants. Such mixing also affects the dynamics of gravity current propagation through the reduction of the density difference that drives the current and the associated increase in height of the flowing layer, and through

the effective drag caused by entrainment of otherwise quiescent ambient fluid. In large-scale gravity currents, the Péclet numbers, which measure the ratio of advective transport to thermal or solute diffusion, are typically extremely large. As a result, effective dilution of a gravity current driven by a density difference due to temperature or dissolved solute can only be achieved through turbulent mixing processes, which transfer the large-scale motion of the gravity current to the small scales at which diffusive mixing operates.

The rate of entrainment of ambient fluid into a flow due to turbulent processes is often modelled as proportional to the difference in velocity between the current and the ambient flow, by dimensional arguments (Morton, Taylor & Turner 1956; Turner 1986). The coefficient of proportionality E is, in general, a function of all the dimensionless groups of the flow, including the density ratio of the current, the Reynolds number and the Péclet number. A typical (but not universal) regime for environmental flows is one in which the density ratio is small (Boussinesq flows), and the Reynolds and Péclet numbers are very large. This leads to a value of E dependent primarily on only one parameter, the Richardson number, which represents the ratio of the stabilizing stratification of the current to destabilizing velocity shear (Turner 1973). Ellison & Turner (1959) determined, from measurements of quasi-steady gravity currents flowing down an incline, that $E(Ri)$ tends to the constant 0.075 as the Richardson number tends to zero, and decays with increasing Richardson number. The currents studied by Ellison & Turner (1959) were of fixed length, flowing from a continuous source of dense fluid into a pool of mixed dense and ambient fluid. When a gravity current is instead led by an advancing flow front, entrainment into the 'head' at the front of the current becomes important, and has been the subject of several experimental studies. Britter and Simpson (Britter & Simpson 1978; Simpson & Britter 1979) used a tank with a flowing ambient and moving floor to bring to rest a gravity current flowing over a horizontal surface, and studied the steady-state transport and mixing of fluid through the current head. Hacker, Linden & Dalziel (1996) used optical measurements of the currents and Hallworth *et al.* (1996) used an acid/base neutralization technique to determine further the interactions between the entraining flow head and the following current. Hallworth *et al.* (1996) calculated a value for the coefficient of entrainment into the head of a gravity current flowing over a solid horizontal surface of $E = 0.063$, similar to the coefficient obtained by Ellison & Turner (1959) for low Richardson number flows.

In this paper, we develop a shallow water model for gravity currents with entrainment that includes the effect of entrainment on the current dynamics and shows that entrainment predominantly occurs in a region close to the front of the current. This feedback of entrainment and dilution on the flow dynamics has previously been studied for currents on an incline, where entrainment occurs readily in laboratory experiments (Ellison & Turner 1959; Britter & Linden 1980; Tickle 1996; Baines 2001; Ross, Dalziel & Linden 2006). We will show that in gravity currents on horizontal surfaces, the effect of entrainment on the current dynamics becomes significant only at long times, which cannot be observed in laboratory-scale currents without the flow becoming dominated by viscous forces (Huppert & Simpson 1980). This accounts for the success of non-entraining models of gravity current propagation arising from the instantaneous release of a volume of dense fluid, which predict that current length grows with time as $t^{2/3}$, in describing laboratory experiments (e.g. Rottman & Simpson 1983). However, for natural-scale flows, the effects of viscosity may remain negligible and thus the dynamics of the motion can become strongly influenced by mixing with environmental fluid. We show that this mixing causes the

long-time structure of the flows generated by instantaneous release of dense fluid ('lock-release currents') and sustained sources to be quite different from their non-entraining counterparts. In particular, the rates at which the currents grow are no longer given by straightforward dimensional reasoning, leading to similarity scalings that apply throughout the current (Hoult 1972), but have a more complex structure in which there are different regions within the current where entrainment plays a more or less important role. In this contribution, we provide the analytical basis for understanding these long-time behaviours and for predicting the spreading rules, and we show explicitly how these results are linked to the form of the entrainment parameterization.

The paper is structured as follows. In § 2, we present the shallow water model with entrainment dependent on Richardson number, for which we provide a derivation in appendix A. In § 3, we find long-time solutions of this model for a current due to an instantaneous release of dense fluid, obtaining a similarity solution of the second kind (cf. Barenblatt 1996). The importance of Richardson number dependence in the entrainment model is highlighted in § 3.2, in which we show that the assumption of a constant entrainment coefficient leads to a different solution structure and current growth rate. In § 4, we find long-time similarity solutions for an entraining current driven by a constant flux, and we again show in § 4.1 that the assumption of a constant entrainment coefficient leads to a different current structure. We examine the effect of entrainment at early times in appendix B by calculating the entrainment-induced perturbations to non-entraining similarity solutions. We summarize the results in § 5 and draw conclusions.

2. Model

We model the gravity current motion using a depth-averaged approach, and derive governing equations for a Boussinesq gravity current flowing over a horizontal surface underneath an deep, incompressible ambient fluid (cf. Parker, Fukushima & Pantin 1986, and others). In appendix A, we show that depth-integration of the incompressible Navier–Stokes equations, and an equation for the transport of a solute by fluid advection and a Reynolds flux, leads to the equations

$$\frac{\partial h}{\partial t} + \frac{\partial}{\partial x}(hu) = w_e, \tag{2.1}$$

$$\frac{\partial}{\partial t}(hu) + \frac{\partial}{\partial x}(hu^2) + \frac{\partial}{\partial x}\left(\frac{g'h^2}{2}\right) = -C_D u|u|, \tag{2.2}$$

$$\frac{\partial}{\partial t}(hg') + \frac{\partial}{\partial x}(hug') = 0, \tag{2.3}$$

where x denotes a horizontal coordinate, t denotes time, u is the horizontal flow velocity, h is the flow height, g' is the flow reduced gravity, C_D is a drag coefficient and w_e is the entrainment velocity. Definitions of these depth-integrated variables are given in appendix A. If there is no entrainment ($w_e = 0$), the reduced gravity g' becomes a constant and (2.1)–(2.3) reduce to the standard shallow water equations (Stoker 1957), which are frequently used to model gravity currents (Ungarish 2009). The drag coefficient C_D represents drag forces other than those caused by entrainment of the stationary ambient fluid, predominantly basal drag, and is typically of the order 10^{-3}–10^{-2} (Hogg & Pritchard 2004). We will show that the effect of this basal
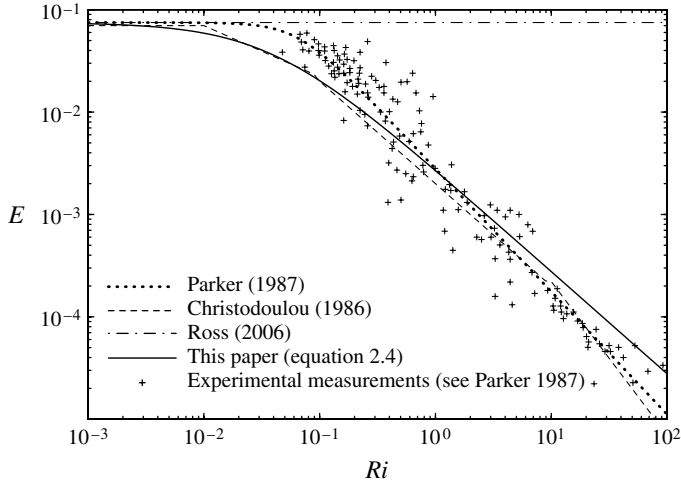
FIGURE 1. Experimental measurements and proposed fits of the dependency of entrainment on the Richardson number. Our simplified dependency (2.4) captures the reduction of entrainment with increasing Richardson number, and the constant entrainment coefficient as $Ri \to 0$. Previous modelling (e.g. Ross *et al.* 2006) has used a constant entrainment coefficient.

drag on the current is often small, and does not affect the structure of the current even at long times.

To close the system, an expression for the entrainment velocity w_e is required. Following Morton *et al.* (1956), we take the rate of entrainment of ambient fluid into a current due to turbulent mixing to be proportional to the difference in velocity between a current and the stationary ambient $|u|$, as indicated by dimensional arguments (Turner 1986); thus $w_e = E |u|$. In Boussinesq, high Reynolds number, high Péclet number flows, Ellison & Turner (1959) determined that the entrainment coefficient E is predominantly a function of the bulk Richardson number $Ri = g'h/u^2$, where $E(Ri)$ tends to a constant, approximately 0.075, for $Ri \ll 1$, and decays at higher Richardson numbers. Subsequent experimental measurements are broadly in agreement with the results of Ellison & Turner (1959) and indicate that entrainment decays approximately as $E \sim Ri^{-1}$ at high Richardson number (figure 1), although there is considerable variation between different experiments (Fernando 1991). Theoretical considerations of the turbulent kinetic energy balance in a gravity current, summarized by Sherman, Imberger & Corcos (1978), suggest a similar dependence of E on Ri, with $E \sim Ri^{-1}$ when $Ri \gg 1$ and $E \sim$ const. when $Ri \ll 1$. We choose a model equation for the dependence of entrainment coefficient on Richardson number that captures the observed behaviour of $E(Ri)$ in both high and low Richardson number regimes, and is of a simple functional form:

$$w_e = E |u| = \frac{E_0}{1 + \psi Ri} |u|. \tag{2.4}$$

With constants $\psi \approx 27$ and $E_0 = 0.075$, this function is a reasonable fit to experimental measurements of entrainment in the literature (figure 1), although the value of ψ is poorly constrained by existing data – and, in particular, may be smaller than this (resulting in increased entrainment) for flows over rough surfaces (Fernandez &

Imberger 2006). When $\psi = 0$, the law reduces to a constant entrainment coefficient $E = E_0$, which has been used to model gravity currents on an incline (Turner 1986; Tickle 1996; Bonnecaze & Lister 1999; Ross *et al.* 2006). Other empirical fits to the experimental data have been proposed (Fernando 1991), and we show those of Parker *et al.* (1987) and Christodoulou (1986) alongside our model (2.4) in figure 1. Importantly, the methods we develop below for analysing the long-time behaviour of currents do not depend strongly upon the precise choice of form of the entrainment model.

The shallow water equations with no entrainment term have frequently been used to model two-dimensional gravity currents spreading over a horizontal surface (Hoult 1972), with a constant Froude number boundary condition ($Fr = u/\sqrt{g'h} \approx 1$) at the flow front, representing the effect on the current of a non-shallow flow 'head' (Benjamin 1968; Huppert & Simpson 1980; Shin, Dalziel & Linden 2004; Marino, Thomas & Linden 2005; Ungarish 2009). The long-time solution of this shallow water model of an instantaneous release of a dense fluid is a 'buoyancy-inertial' similarity solution, where, in terms of the reduced gravity g' and a constant volume per unit width V, both dependent on the initial conditions, the current length x_f varies as $(g'Vt^2)^{1/3}$, current velocity $u \sim (g'V/t)^{1/3}$ and current height $h \sim (V^2/g't^2)^{1/3}$. The existence of this buoyancy-inertial regime has been verified by laboratory experiments (Rottman & Simpson 1983) and emerges as an attracting similarity solution to the underlying model equation (Mathunjwa & Hogg 2006). However, substituting these scalings into the mass equation for an entraining gravity current (2.1) and (2.4), we find that the terms $\partial h/\partial t$ and $\partial(hu)/\partial x$ scale as $(V^2/g't^5)^{1/3}$, whereas the entrainment term w_e scales as $E_0(Vg'/t)^{1/3}$. At large times (when $t \gg \tau$, where $\tau \sim (V/(g'^2 E_0^3))^{1/4}$), the entrainment term then becomes unbalanced in (2.1). Thus, at sufficiently long times, currents in the buoyancy-inertia regime must transition to a new solution in which entrainment forms part of the dominant balance, even if the rate of entrainment (governed by E_0) is small. In laboratory experiments, the transition to a viscous-buoyancy similarity regime (Huppert & Simpson 1980) may occur before entrainment becomes significant, preventing observation of the entraining regime. However, in larger-scale natural flows, where the onset of viscous effects occurs much later, the entraining solution that we describe may describe the predominant flow regime of the current.

Ross *et al.* (2006) showed that equations similar to (2.1)–(2.3), with a constant entrainment coefficient, and extended to include the effect of a finite incline, admit a similarity solution for a finite release of dense fluid, in which the current length $x_f \sim t^{2/3}$, $h \sim t^{2/3}$ and $g' \sim t^{-4/3}$ (here, for clarity, we have dropped the factors that render these relationships dimensionally consistent). Ross *et al.* (2006) argued that this solution is valid only above a critical slope angle; in §3.2, we extend this solution to the case of a horizontal gravity current and show how the structure of the similarity solution and the spreading rule is changed.

The buoyancy conservation equation (2.3) implies that

$$\frac{\mathrm{d}}{\mathrm{d}t} \int_0^{x_f} g'h \, \mathrm{d}x = (hug')_{x=0}, \tag{2.5}$$

where, for kinematic consistency,

$$\frac{\mathrm{d}x_f}{\mathrm{d}t} = u(x_f, t). \tag{2.6}$$

For a current generated by the instantaneous release of dense fluid, with a barrier (or plane of symmetry) imposing the boundary condition $hug' = 0$ at $x = 0$, the total buoyancy of the current B_0 is constant, which implies that

$$\int_0^{x_f} g'h \, dx = B_0. \tag{2.7}$$

When $u(0, t) = 0$, and provided that $h(0, t) > 0$, the characteristic equation

$$\frac{dg'}{dt} = -\frac{Eg'u}{h} \quad \text{on} \quad \frac{dx}{dt} = u \tag{2.8}$$

reduces to $(\partial g'/\partial t)_{x=0} = 0$; that is, the excess density at the back of the current is constant.

For a current driven by a sustained flux, we specify the buoyancy flux $Q_B = (hug')_{x=0}$ and reduced gravity $g'_0 = g'(0, t)$ at the inflow, both constants. (We note that imposing only two boundary conditions assumes that the flow at $x = 0$ is subcritical; at sufficiently large times, this is the case for the similarity solutions found in this paper.) Further imposing $x_f(0) = 0$, we obtain

$$\int_0^{x_f} g'h \, dx = Q_B t. \tag{2.9}$$

At the front of the current, we apply a constant Froude number condition,

$$\frac{dx_f}{dt} = u(x_f, t) = Fr_0 \left(\sqrt{g'h} \right)_{x=x_f}, \tag{2.10}$$

where Fr_0 is a constant that is close to unity (Huppert & Simpson 1980; Shin *et al.* 2004). For the purposes of our computations, we adopt $Fr_0 = 1$ (Shin *et al.* 2004), although it will be shown that the value of the Froude number does not strongly influence the structure of the solutions.

To study the effect of entrainment on solutions of the governing equations (2.1)–(2.3), we introduce checked ($\check{}$) dimensionless variables that have scales based on the onset time of entrainment, defined as

$$\{x, t, h, u, g'\} = \left\{ \left(\frac{B_0}{g'_0 E_0} \right)^{1/2} \check{x}, \left(\frac{B_0}{g'^3_0 E^3_0} \right)^{1/4} \check{t}, \left(\frac{B_0 E_0}{g'_0} \right)^{1/2} \check{h}, \left(B_0 g'_0 E_0 \right)^{1/4} \check{u}, g'_0 \check{g}' \right\} \tag{2.11}$$

in the case of a constant buoyancy lock-release, and as

$$\{x, t, h, u, g'\} = \left\{ \frac{Q_B^{2/3}}{g'_0 E_0} \check{x}, \frac{Q_B^{1/3}}{g'_0 E_0} \check{t}, \frac{Q_B^{2/3}}{g'_0} \check{h}, Q_B^{1/3} \check{u}, g'_0 \check{g}' \right\} \tag{2.12}$$

in the case of a current driven by a constant flux. In both situations, (2.1)–(2.3) become

$$\frac{\partial \check{h}}{\partial \check{t}} + \frac{\partial}{\partial \check{x}} \left(\check{h} \check{u} \right) = \frac{|\check{u}|}{1 + \psi \left(\check{g}' \check{h} / \check{u}^2 \right)}, \tag{2.13}$$

$$\frac{\partial}{\partial \check{t}} \left(\check{h} \check{u} \right) + \frac{\partial}{\partial \check{x}} \left(\check{h} \check{u}^2 \right) + \frac{\partial}{\partial \check{x}} \left(\frac{\check{g}' \check{h}^2}{2} \right) = -\frac{C_D}{E_0} \check{u} |\check{u}|, \tag{2.14}$$

$$\frac{\partial}{\partial \check{t}} \left(\check{h} \check{g}' \right) + \frac{\partial}{\partial \check{x}} \left(\check{h} \check{u} \check{g}' \right) = 0, \tag{2.15}$$

with boundary conditions $\check{g}' = 1$ and $\check{h}\check{u} = 1$ at $\check{x} = 0$ for the case of constant flux, and $\check{g}' = 1$ and $\check{g}'\check{h}\check{u} = 0$ at $\check{x} = 0$ with an initial condition that satisfies $\int_0^{\check{x}_f} \check{h}\check{g}' \, d\check{x} = 1$ in the case of constant buoyancy. We note that with these non-dimensionalizations, in which scales are based on the onset time of entrainment rather than on the current initial conditions, the non-dimensional initial conditions depend on E_0, scaling as $\check{x}_f \sim E_0^{1/2}$ and $\check{h} \sim E_0^{-1/2}$, and that the governing equations feature only the parameters C_D/E_0 and ψ. This choice of dimensionless variables is advantageous for the analysis that follows. However, in the limit of vanishing E_0, which corresponds to the solutions when $t \ll 1$, these early-time scalings result in the right-hand side of (2.13) becoming negligible, and the non-entraining shallow water model for gravity currents (Rottman & Simpson 1983) is recovered. Henceforth, we use the dimensionless version of the model (2.13)–(2.15), and for clarity we drop the checks.

2.1. *Numerical solution of the model*

The model (2.13)–(2.15) is a system of hyperbolic conservation laws, which can be solved numerically by a wide variety of techniques (LeVeque 2002; Toro 2009); we use the method of Kurganov & Tadmor (2000), a semi-discrete non-oscillatory central scheme, with a WENO limiter to prevent spurious oscillations at any shocks that form in the solution. We solve the equations numerically using rescaled spatial coordinate $y = x/x_f(t)$, which simplifies the flow domain to $0 \leqslant y \leqslant 1$. To apply the constant Froude number boundary condition at $y = 1$, we augment the vector of unknowns resulting from the spatial discretization of the conservation laws (Kurganov & Tadmor 2000) with four additional variables: x_f, and the solution variables h, u and g' at $x = x_f$. The temporal evolution of these frontal variables is governed by the four ordinary differential equations $d/dt\,(Fr_0) = 0$, the kinematic condition (2.6), the characteristic equation (2.8) and a further characteristic equation associated with characteristics moving at speed $u + \sqrt{g'h}$. We apply the values of h, u and g' at $x = x_f$ thus obtained as boundary conditions at $y = 1$ in the spatially discretized problem.

A numerical solution of the governing equations (2.13)–(2.15) representing an instantaneous lock-release gravity current is shown in figure 2 for times up to $t = 50$. The parameters $Fr_0 = 1$, $\psi = 27$ are chosen to reflect experimentally measured values, and we choose $C_D/E_0 = 0$ and an initial lock aspect ratio of 1:1 in dimensional variables. At early times there is very little entrainment into the current, but by $t = 50$ entrainment has reduced the excess density at the current front to $\sim 13\,\%$ of its initial value. This entrainment has relatively little effect on the current dynamics at the times illustrated in figure 2; the effective drag caused by acceleration of stationary ambient fluid that is entrained into the current results in a current length at $t = 50$ that is approximately $8\,\%$ less than that of an equivalent non-entraining current. In appendix B, we quantify these effects at early times ($t \lesssim 30$) by calculating the perturbations to the non-entraining buoyancy-inertial similarity solution that result from entrainment. These calculations bring out the important features of entrainment, which are that there is most mixing close to the front, leading to a current that is both deeper and slower than the non-entraining counterparts.

At later times, however, entrainment is no longer a perturbation to the non-entraining flow, but instead plays a leading-order role in current dynamics. This implies that the early-time perturbations in appendix B no longer capture the motion and so a different approach is required. The current length x_f and two measures of the dilution of the current, the total current volume $\int_0^{x_f} h \, dx$ and reduced gravity at the
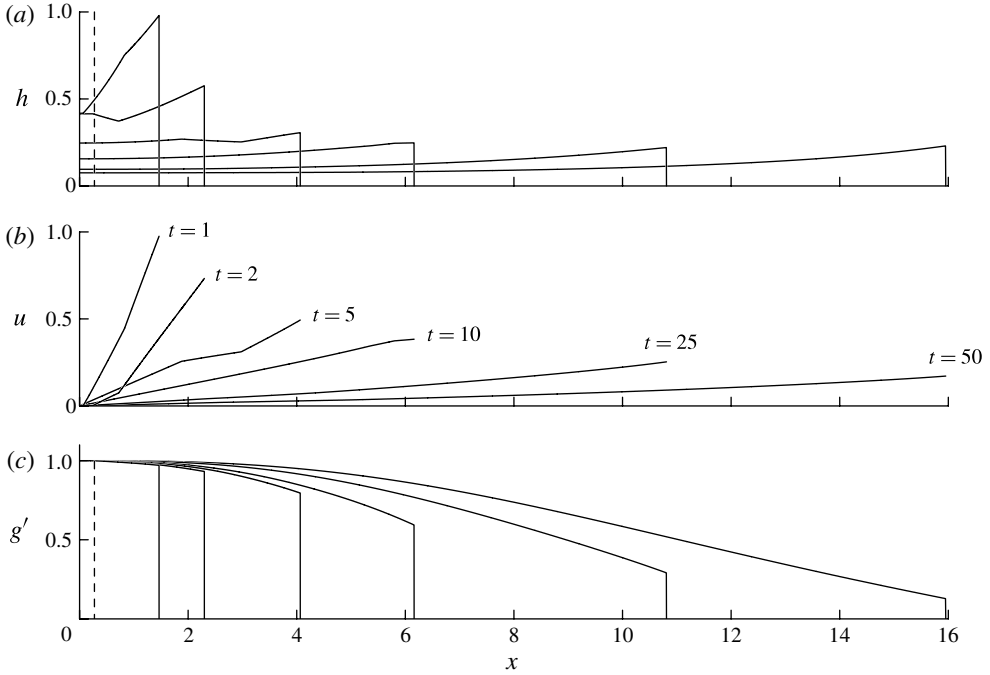
FIGURE 2. The height $h(x, t)$, velocity $u(x, t)$ and reduced gravity $g'(x, t)$ as functions of distance for an entraining gravity current with $\psi = 27$, $Fr_0 = 1$ and $C_D/E_0 = 0$ at $t = 1, 2, 5, 10, 25, 50$. The initial conditions represent the instantaneous release of a lock of dense fluid with aspect ratio 1 ($h = 1/\sqrt{E_0}$, $g' = 1$ for $0 \leqslant x \leqslant \sqrt{E_0}$, $h = g' = 0$ elsewhere, $u = 0$ everywhere), and are indicated with dashed lines.

current front $g'(x_f, t)$, are plotted as functions of time in figure 3, both for $\psi = 27$, $Fr_0 = 1$ and $C_D/E_0 = 0$, as used in figure 2, and for the same entrainment law and front condition but with a non-zero drag coefficient $C_D/E_0 = 0.1$. In both cases, up to $t \approx 20$ the current volume remains close to its initial value, indicating relatively small amounts of entrainment, and the growth of the current is in agreement with existing theory and laboratory experiments (e.g. Rottman & Simpson 1983), with an initial adjustment phase, where $(x_f - x_0) \sim t$, transitioning to a buoyancy-inertial phase in which $x_f \sim t^{2/3}$. By $t = 100$, the front of the current is substantially diluted, and for larger times a new regime is established in which x_f scales as a power of t that is dependent on the parameters C_D/E_0, Fr_0 and ψ; in particular, as $t^{0.447}$ for the current without basal drag and as $t^{0.412}$ for the current with $C_D/E_0 = 0.1$. The onset time of this new regime is dependent on ψ, Fr_0 and C_D/E_0, in particular, occurring sooner as C_D/E_0 increases. The onset of this late-time regime is illustrated by the plots in figure 3(a) of the current front position x_f rescaled by its late-time behaviour $x_f/(ct^\gamma)$, and by the plots in figure 3(c) of the gradient of the log–log plot of x_f against t, $d \log(x_f)/d \log(t)$, which indicate that the current with $C_D/E_0 = 0.1$ is close to its late-time behaviour by $t = 160$. Although the late-time power-law exponent γ is dependent on ψ, Fr_0 and C_D/E_0, it is independent of the initial conditions: it is this variation of the power-law exponents that we explain in the next section.

We note that, for sufficiently large times, viscous effects become significant even in very large currents. The time at which viscosity starts to affect flows in the buoyancy-
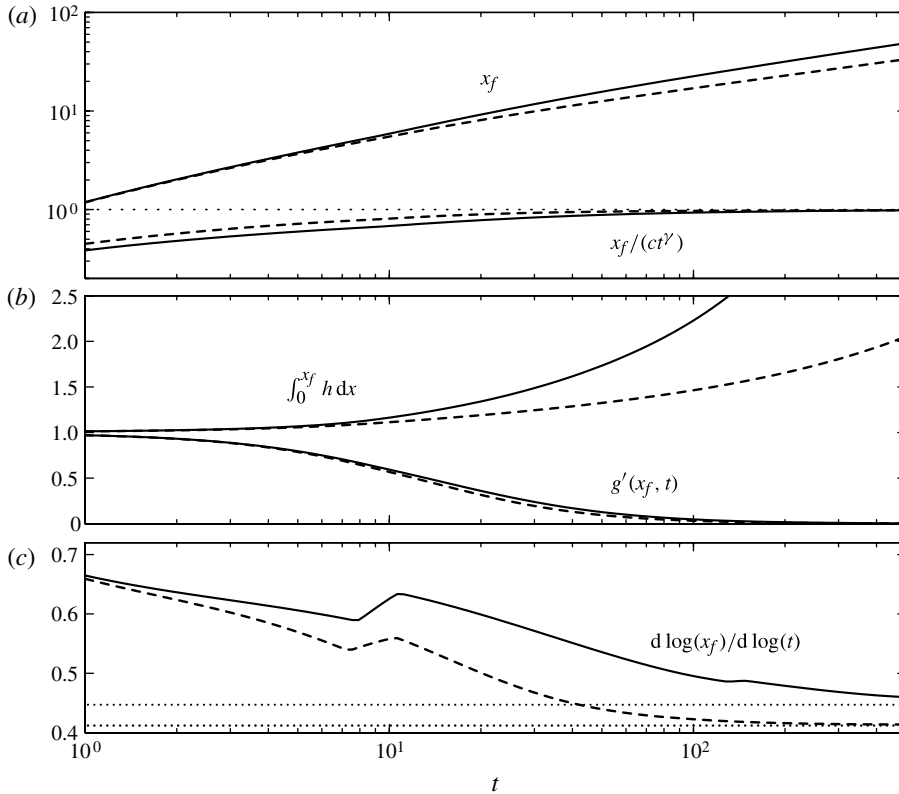
FIGURE 3. The time-evolution of entraining density currents generated by a lock-release initial condition, determined from time-dependent numerical solutions of the governing equations, with parameters $\psi = 27$, $Fr_0 = 1$ and $C_D/E_0 = 0$ (solid lines) and $C_D/E_0 = 0.1$ (dashed lines). (*a*) The front position x_f as a function of time. At large times, the current with $C_D/E_0 = 0$ grows as $x_f \sim c_1 t^{0.447}$ and the current with $C_D/E_0 = 0.1$ grows as $x_f \sim c_2 t^{0.412}$. The approach to these long-time behaviours is indicated in the plot of $x_f/(ct^\gamma)$ (where $\gamma = 0.447$ for the solid curve representing $C_D/E_0 = 0$ and $\gamma = 0.412$ for the dashed curve representing $C_D/E_0 = 0.1$). (*b*) Reduced gravity at the flow front $g'(x_f, t)$ and the total current volume as functions of time. (*c*) The quantity $d \log(x_f)/d \log(t)$, which can be interpreted as the gradient of the log–log plot of x_f against t in (*a*). The dotted lines indicate the values 0.447 (top) and 0.412 (bottom), the long-time limits of the currents with $C_D/E_0 = 0$ and $C_D/E_0 = 0.1$, respectively.

inertial is regime is given by Huppert ([1982](#)), and in our non-dimensionalized variables is as follows:

$$t_v = V^{9/28} \eta^{-3/7} g'^{3/14} E_0^{3/4}, \tag{2.16}$$

where η is the kinematic viscosity of the fluid and V is the volume per unit width of initial lock-release. Evaluating this expression with values suitable for a submarine current ($\eta = 10^{-6}$ m^2 s^{-1}, $g' = 1$ m s^{-2}, $E_0 = 0.075$) indicates that viscosity can be neglected for $t < 53$ in currents with an initial lock length scale $V^{1/2}$ of 1 m, for $t < 150$ in currents with an initial length scale of 5 m and for $t < 235$ in currents with an initial length scale of 10 m. Currents with drag and entrainment parameterized

by $C_D/E_0 = 0.1$ and $\psi = 27$ reach the entraining similarity regime at $t \approx 160$ (figure 3), confirming that, while entrainment will act only as a small perturbation to laboratory-scale flows (detailed in appendix B), large-scale environmental flows may well be governed by the entraining regime that we now describe.

3. Similarity solutions for a lock-release gravity current

We seek similarity solutions to the equations governing the evolution of an entraining gravity current (2.13)–(2.15) in the case of a lock-release current at long times, when entrainment plays a non-negligible role. To this end, we write general similarity forms for the dependent variables,

$$x_f = ct^\gamma, \quad h = ct^\alpha H(y), \quad g' = ct^\beta G(y) \quad \text{and} \quad u = ct^{\gamma-1}U(y), \tag{3.1}$$

where $y = x/x_f$. The constant exponents α, β and γ, similarity functions $H(y)$, $G(y)$ and $U(y)$ and constant c are to be determined as part of the solution. We find that the boundary condition of constant $g' = g'_0$ at $x = 0$ (2.8) cannot be satisfied simultaneously with a scaling that allows the entrainment term in (2.13) to remain balanced with the other terms. This means that there cannot be a straightforward similarity solution but, rather, a more complicated structure, which will nevertheless be shown to admit a self-similar solution in the bulk of the flow. Given that the only mismatch occurs at the rear boundary ($x = 0$), we let (3.1) represent the scalings of an outer region, comprising the bulk of the current, and introduce a second set of scalings,

$$x_c = ct^C, \quad h = ct^A\hat{H}(\eta), \quad g' = c\hat{G}(\eta) \quad \text{and} \quad u = ct^{C-1}\hat{U}(\eta), \tag{3.2}$$

where $\eta = x/x_c$, in an 'inner' region near the boundary at $x = 0$. Here, A and C are constant exponents and $\hat{H}(\eta)$, $\hat{G}(\eta)$ and $\hat{U}(\eta)$ are similarity functions within the inner region.

To match the constant Froude number condition at the current front, we scale the Froude number to be independent of time in the outer region; this implies $\alpha + \beta - 2(\gamma - 1) = 0$. Furthermore, we look for solutions where the entrainment term in (2.13) is in balance with the other terms in the outer region: since the Richardson number in the outer region does not depend on time, this gives $\gamma = \alpha$. By contrast, the Richardson number in the inner region grows with time, which validates the assumption of subcritical inflow at large times needed when applying two boundary conditions at $x = 0$. This increasing Richardson number also implies that $\partial(g'h^2/2)/\partial x$ has nothing to balance it in (2.14) and therefore that $g'h^2$ is constant in the inner region, to leading order at large times: matching then suggests that $g'h^2$ should be scaled in the same way in both the inner and outer solutions, i.e. $2A + B = 2\alpha + \beta$. Finally, by imposing a constant total buoyancy (2.7), we obtain $\max(\alpha + \beta + \gamma, A + C) = 0$. This can only be satisfied if $A + C = 0$ with $\alpha + \beta + \gamma < 0$, meaning that, at large times, the total buoyancy of the current is contained almost entirely in the inner region. Thus we have a current with an extensive bulk outer region, within which mixing with the ambient fluid is important and fluid inertia and the hydrostatic pressure gradient dominate the dynamics, matched to a relatively quiescent inner region close adjacent to the rear boundary, within which entrainment plays only a relatively weak role. Although of negligible extent, it is the inner region that provides the dominant contribution to the overall buoyancy.

Prescribing these constraints on the time dependencies of the similarity form of the dependent variables, we obtain a system in which the scaling exponents are not

determined *a priori*, but have one undetermined parameter. Writing the scalings in terms of the current growth exponent γ, we have $\alpha = \gamma$, $\beta = \gamma - 2$, $A = 3\gamma/2 - 1$ and $C = -3\gamma/2 + 1$. In the outer region, denoting differentiation with respect to y by a prime, the ordinary differential equations governing the similarity variables are then

$$\gamma H - \gamma y H' + (HU)' = \frac{U}{1 + \psi \dfrac{GH}{U^2}}, \tag{3.3}$$

$$(2\gamma - 1)HU - \gamma y(HU)' + \left(HU^2 + \frac{1}{2}GH^2\right)' = -\frac{C_D}{E_0}U^2, \tag{3.4}$$

$$(2\gamma - 2)HG - \gamma y(HG)' + (HUG)' = 0. \tag{3.5}$$

The boundary conditions at $y = 0$ are obtained by matching the outer solution to the inner; in applying these conditions at $y = 0$, we suppose that the inner region grows more slowly than the outer region; that is, $C < \gamma$. This inequality implies $\gamma > 2/5$, and that $U \to 0$ as $y \to 0$. At the front of the current we impose the kinematic condition $U(1) = \gamma$ and Froude number condition $U(1) = Fr_0^2 G(1)H(1)$.

With this kinematic condition, (3.5) becomes singular at $y = 1$. It is therefore instructive to consider the power series of the equations about this point, and letting $s = 1 - y$, we construct a power series of the form

$$H = H_0 + H_1 s + \cdots, \quad U = U_0 + U_1 s + \cdots \quad \text{and} \quad G = G_0 + G_1 s + \cdots. \tag{3.6}$$

Substituting into (3.3)–(3.4), an additional boundary condition is obtained from the coefficients of the constant terms, $H_0 = \gamma Fr_0^2/(2 - \gamma)(Fr_0^2 + \psi)$. We thus have four boundary conditions to impose on the third-order boundary value problem (3.3)–(3.5) with unknown parameter γ, and we numerically integrate it using a shooting technique.

The solution of this eigenvalue problem is shown in figure 4. The growth exponent eigenvalue γ varies with the entrainment law parameter ψ (figure 4a), although the dependence is remarkably weak; over a range of ψ between 1 and 1000 (centred around the experimentally inferred value $\psi = 27$), the current growth rate $\gamma \approx 0.447$ varies only by $\sim 3\%$. While the dependence on ψ is weak, the difference between the current growth rate with no entrainment ($t^{2/3}$) and that predicted by our model is significant.

The eigenfunctions at $\psi = 27$ (figure 4b) are typical of those obtained. The buoyancy force GH^2 is almost constant throughout most of the current, where the Richardson number is large (quiescent flow) and the entrainment small. Near the front of the current, the flow height H is greater than that in the bulk of the current, and the entrainment coefficient is greatest. The current velocity U is slightly less than that of a linearly expanding current (which would have $U = \gamma y$), indicating that fluid near the front of the current is transported into the flow 'tail'. This structure for a lock-release current, with a flow head in which entrainment is important and a tail region supplied with fluid left behind by the head, is consistent with the structure found at late times in experimental lock-release currents (Hallworth *et al.* 1996).

3.1. *Similarity structure of the current*

Similarity solutions are commonly obtained as the long-time solutions of PDEs governing physical systems. If the scalings associated with these similarity solutions can be obtained directly, either from dimensional analysis alone or through scaling of
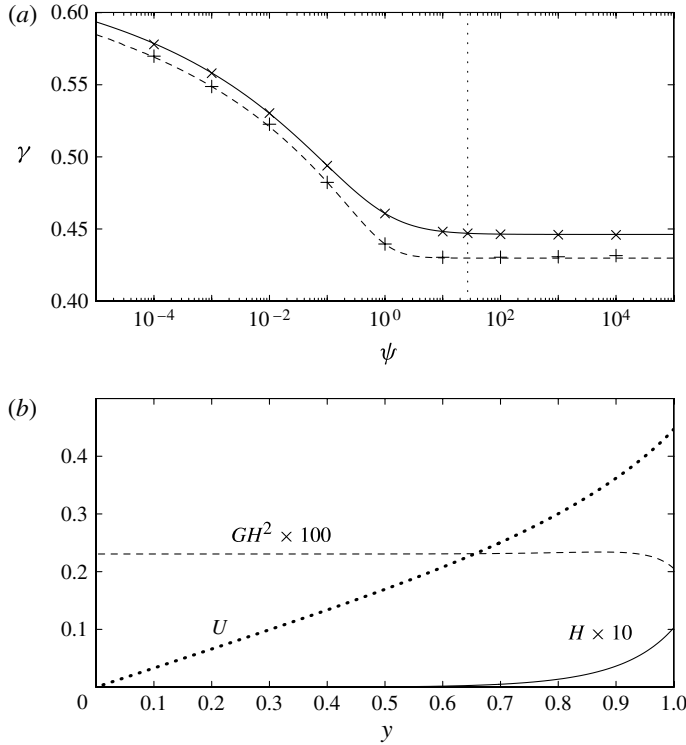
FIGURE 4. (*a*) The current growth exponent, γ, as a function of ψ. The solid line indicates values calculated from solutions of the similarity eigenvalue problem (3.3)–(3.5); crosses (×) indicate values calculated from time-dependent numerical solutions at very large times. The dashed line and plus signs (+) illustrate the corresponding growth exponents using the entrainment law (3.7) proposed by Parker *et al.* (1987). The vertical dotted line shows the experimentally inferred value $\psi = 27$. (*b*) The current height H, velocity U and GH^2 in similarity variables, calculated from a solution of (3.3)–(3.5) for $\psi = 27$.

the governing equations, the solution is known as a similarity solution of the first kind. Frequently, the multiplicative constant applied to the scalings (c, in (3.1)) can then be determined by solving the similarity equations and making use of a conserved quantity in the system. In the similarity solution for the entraining gravity current derived in this section, the similarity scalings are not determined from inspection of the equations but, instead, by solution of an eigenvalue problem. This is a characteristic of self-similar solutions of the second kind (Barenblatt 1996), which also have the property that the multiplicative constant cannot be determined globally, but is instead dependent on the initial conditions of the problem and the time-dependent approach to similarity. This behaviour is observed in time-dependent numerical solutions of the governing equations (2.13)–(2.15). Long-time growth exponents are determined from time-dependent solutions, such as the results of the numerical computations plotted in figure 3, by extending these computations to very long times and numerically evaluating the gradient of $\log(x_f)$ against $\log(t)$, which approaches the constant growth exponent at large times (figure 3*c*). These calculations, indicated by the crosses in figure 4(*a*), match those predicted by the similarity solution, suggesting that the similarity solution described is realized by the system at large times.
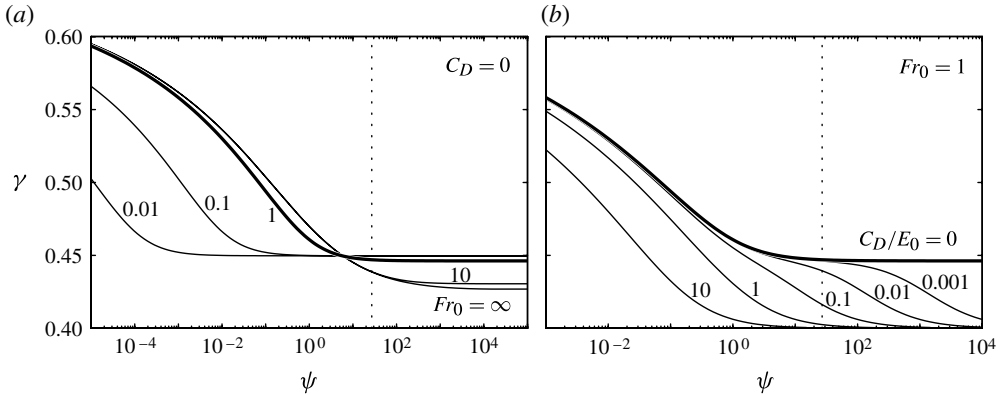
FIGURE 5. The dependence of the current growth exponent γ on (a) ψ and the frontal Froude number Fr_0 at $C_D = 0$, and (b) ψ and C_D at $Fr_0 = 1$, for a current generated by the instantaneous release of a fixed volume of dense fluid. The thick line common to both plots (and to figure 4) illustrates the case $Fr_0 = 1$, $C_D = 0$. The vertical dotted lines illustrate the value $\psi = 27$ fitted from experimental measurements.

The structure found for entraining 'lock-release' currents, in which the current scalings are dependent on γ and scalings in a region near $x = 0$ differ from those near the current front, is insensitive to the exact formulation of the entrainment law. The growth rate of similarity solutions calculated with an entrainment rate of the form suggested by Parker *et al.* (1987),

$$E_{parker}(Ri) = \frac{0.075}{\sqrt{1 + \psi^2 Ri^{2.4}}}, \tag{3.7}$$

is illustrated in figure 4(a) with a dashed line, and is similar to those obtained with the simple entrainment law (2.4).

The effect of the frontal Froude number Fr_0 on the current growth rate is illustrated in figure 5(a). When $\psi \approx 27$, the current growth rate is remarkably insensitive to the frontal Froude number Fr_0, varying by less than 2 % within the range $Fr_0 = 0.5$–2. We note that in the limit $Fr_0 \to \infty$ (which is applied when modelling shallow free-surface flows, and here corresponds to the boundary condition $g' = 0$ at the current front), the current structure is unchanged and the growth rates are similar to those at $Fr \approx 1$. This is in contrast to solutions of the non-entraining shallow water equations, in which finite and infinite Froude number conditions at the flow front result in qualitatively different behaviour (Hogg 2006).

The effect of basal drag on the current, parameterized through the coefficient C_D, is shown in figure 5(b). At physically realistic values of $C_D/E_0 = 10^{-2}$ to 10^{-1}, the predicted growth exponent of the current is decreased slightly from the value observed for $C_D = 0$ to approximately 0.42 to 0.44. In the limit $\psi \to \infty$, for finite C_D the growth exponent α tends to $2/5$ from above. In this limit, the scalings in the inner region tend to those of a non-entraining drag-dominated current (Hogg & Woods 2001).

3.2. *Constant entrainment coefficient*

When the entrainment coefficient is taken to be constant (i.e. $\psi = 0$, which is a simplification made in previous studies, e.g. Ross *et al.* 2006), the current structure

differs from that in the $\psi > 0$ case above when the coefficient is dependent on the Richardson number. Applying the same conditions to the scalings of inner and outer variables as before, and specifying that the entrainment coefficient is constant in (2.13), implies that within the 'inner' region there is an additional constraint arising from imposing a balance between the entrainment flux $E|u|$, with its now constant coefficient, and the other terms $\partial h/\partial t$ and $\partial(hu)/\partial x$. This additional constraint, which implies $A = C$, is necessary to avoid the entrainment term becoming larger than the other two and, together with the constraints obtained earlier, uniquely determines the scalings. We find that $x_f = t^{2/3}$, $u \sim t^{-1/3}$, $h \sim t^{2/3}$ and $g' \sim t^{-4/3}$ in the outer region, while within the inner, $x_c, g', h \sim 1$ and $u \sim t^{-1}$. Under these scalings, $xg'h \sim 1$ in both the inner and the outer regions and so we cannot identify which region, if either, contributes dominantly to the integral expression for the conservation of buoyancy.

Using these outer scalings, and integrating (3.5) subject to the boundary condition $U(1) = 2/3$, gives $U = 2y/3$. Equation (3.3) then gives $H = y/2$ and (3.4), with the boundary condition $G = 0$ at $y = 1$, then gives $G = (8/9)((1 + Fr_0^{-2})y^{-2} - y)$. This outer solution is a special case of the solution presented for flows on an incline by Ross *et al.* (2006). We note that G diverges as $y \to 0$ and evidently does not satisfy the required boundary condition $G(0) = t^{4/3}$. While this difficulty may be rectified by introducing a boundary layer region close to the back wall ($x = 0$), the buoyancy integral in bulk of the flow $\int_\delta^1 HG \, dy$ continues to diverge logarithmically. This observation suggests that logarithmic corrections to the straightforward similarity solution may be required, and this is indeed what we establish below.

We introduce the following expressions for the velocity, height and reduced gravity field:

$$h = x_f \tilde{H}(y, t), \quad u = \dot{x}_f \tilde{U}(y, t) \quad \text{and} \quad g' = \frac{\dot{x}_f^2}{x_f} \tilde{G}(y, t), \qquad (3.8)$$

where $x_f = t^{2/3} \Lambda(t)$. At long times ($t \gg 1$), we construct solutions where

$$\tilde{U}(y, t) = \tilde{U}_0(y) + \cdots, \quad \tilde{H}(y, t) = \tilde{H}_0(y) + \cdots \quad \text{and} \quad \tilde{G}(y, t) = \tilde{G}_0(y) + \cdots, \quad (3.9)$$

and $t \, d\Lambda/dt \ll \Lambda$, a condition that will be shown to hold in what follows. We substitute these expressions in the governing equations (2.13)–(2.15) and apply boundary conditions at the front of the current ($\tilde{U}_0 = 1$, $\tilde{U}_0 = Fr_0(\tilde{G}_0 \tilde{H}_0)^{1/2}$ at $y = 1$), to find that

$$\tilde{U}_0 = y, \quad \tilde{H}_0 = \frac{y}{2} \quad \text{and} \quad \tilde{G}_0 = 2\frac{(1 + Fr_0^{-2} - y^3)}{y^2}. \qquad (3.10)$$

Up to the different pre-factor of g' in (3.8), these are identical to the solutions established by Ross *et al.* (2006). These solutions do not satisfy the boundary condition at $y = 0$, namely $\tilde{G} = x_f/\dot{x}_f^2$, and so we examine the governing equations within a small region of size $y \sim \delta = \dot{x}_f/x_f^{1/2}$ close to the back wall at $y = 0$. To this end, we introduce a rescaled spatial coordinate, $Y = y/\delta$, and seek solutions of the form

$$\tilde{H} = \delta \bar{H}_0 + \cdots, \quad \tilde{U} = \delta \bar{U}_0 + \cdots \quad \text{and} \quad \tilde{G} = \delta^{-2} \bar{G}_0 + \cdots, \qquad (3.11)$$

where the distinguished scalings for these 'inner' variables are determined by matching to the bulk of the current. The most important term in the leading-order governing equations within the inner region comes from the momentum equation, which asserts

that

$$\frac{\partial}{\partial Y} \left(\bar{H}_0^2 \bar{G}_0 \right) = 0. \tag{3.12}$$

This is entirely similar to the matching procedure and the leading-order dynamics of current governed by a variable entrainment coefficient (§ 3). Matching then enforces

$$\bar{H}_0^2 \bar{G}_0 = \frac{1}{2} \left(1 + \frac{1}{Fr_0^2} \right). \tag{3.13}$$

Finally, we are in a position to enforce the conservation of buoyancy, which in this case has contributions from both the bulk of the flow and the 'inner' region. This integral may be evaluated to leading order by splitting it into separate contributions

$$\dot{x}_f^2 x_f \left[\frac{1}{\delta} \int_0^{\delta^\mu} \bar{H}_0 \bar{G}_0 \, dy + \int_{\delta^\mu}^1 \tilde{H} \tilde{G} \, dy \right] = 1, \tag{3.14}$$

where μ is an arbitrary constant ($\mu > 1$): we anticipate that the final expression must be independent of μ to leading order. First, in the outer region, we find that

$$\int_{\delta^\mu}^1 \tilde{H}_0 \tilde{G}_0 \, dy = \left(1 + \frac{1}{Fr_0^2} \right) \mu \log \frac{1}{\delta} - \frac{1}{3} + \frac{\delta^{3\mu}}{3}. \tag{3.15}$$

In the inner region, using (3.13),

$$\int_0^{\delta^\mu} \bar{H}_0 \bar{G}_0 \, dy = \int_0^{\delta^{\mu-1}} \frac{1}{2\bar{H}_0} \left(1 + \frac{1}{Fr_0^2} \right) dY. \tag{3.16}$$

Since $H_0(Y) = O(1)$ for $Y = O(1)$, its contribution to the integral is of $O(1)$ magnitude and we cannot evaluate it without further knowledge of the solution in the inner region. However, this term is subdominant; $H_0 \sim Y/2$ as $Y \to \infty$ by matching, so the $Y \gg 1$ part of the integral makes an $O(\log \delta)$ contribution, namely

$$\int_0^{\delta^{\mu-1}} \frac{1}{2\bar{H}_0} \, dY = \left(1 + \frac{1}{Fr_0^2} \right) (1 - \mu) \log \frac{1}{\delta} \quad (+ O(1) \text{ terms}). \tag{3.17}$$

Hence, combining these results, we find that to leading order,

$$\dot{x}_f^2 x_f \left(1 + Fr_0^{-2} \right) \log \frac{1}{\delta} = 1, \tag{3.18}$$

which, as expected, is independent of μ. To complete this evaluation and determine Λ, we now substitute the leading-order expression for $\delta = (3/2)t^{-2/3}$ and thus when $t \gg 1$,

$$x_f \sim \frac{3}{2} \left(\frac{t^2}{(1 + Fr_0^{-2}) \log t} \right)^{1/3}. \tag{3.19}$$

This asymptotic long-time solution represents a logarithmic correction to the straightforward similarity solution (for which $x_f \sim t^{2/3}$), and shows good agreement with the front position found from direct time-integration of the governing equations (2.13)–(2.15) (figure 6).
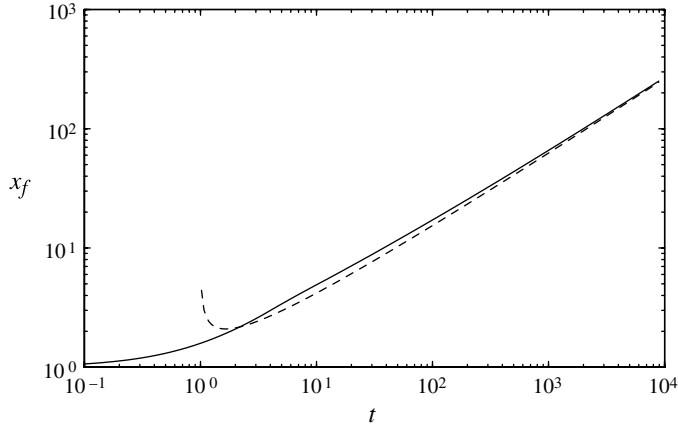
FIGURE 6. The dimensionless front position x_f as a function of time for an entraining density current with constant buoyancy and $\psi = 0$, with $Fr_0 = 1$, $C_D = 0$, determined from time-dependent numerical solutions of the governing equations (solid line). The long-time asymptotic solution given by (3.19) is indicated by a dashed line.

4. Similarity solutions for a current generated by a continuous source

For gravity currents due to a constant flux of buoyancy, the non-entraining shallow water model admits a solution with finite Froude number condition at the current front, in which the current expands linearly ($x_f \sim t$) and the flow height and velocity take constant values throughout the current (see, e.g., Gratton & Vigo 1994). As with currents caused by an instantaneous release of dense fluid, the addition of entrainment to the model of such a current has a relatively small effect on the dynamics at sufficiently early times (figure 7). At these early times, the velocity and height of the current are approximately uniform, as suggested by the non-entraining solution, but entrainment into the body of the current results in a decrease in the reduced gravity of the current, a small increase in current height and a corresponding decrease in velocity. These early-time features exactly parallel those effects observed for currents generated by an instantaneous release of dense fluid. They may be analysed while they are small perturbations using the techniques of appendix B.

The front position x_f increases more slowly than the linear growth found in the non-entraining case, and at larger times approaches the growth rate $x_f \sim t^{4/5}$ (illustrated in figure 8), where, as with currents caused by an instantaneous release of fluid, the entraining regime is reached at $t \approx 150$. Unlike in currents caused by an instantaneous release of fluid, where the growth rate exponent was a function of the problem parameters, in the case of currents fed by a constant flux of buoyancy, the growth rate exponent is fixed at 4/5 and only the constant of proportionality is dependent on the parameters ψ, C_D/E_0 and Fr_0.

The similarity scalings for a current driven by a constant buoyancy flux are derived in a similar manner to a current caused by an instantaneous release of fluid. With a constant flux of buoyancy, the total current buoyancy now increases linearly, implying the relationship $\max(\alpha + \beta + \gamma, A + C) = 1$ in the scalings (3.1)–(3.2). In the case of the current due to an instantaneous release, entrainment was found to be unimportant in the inner region. Making the same assumption in the case of constant flux, and
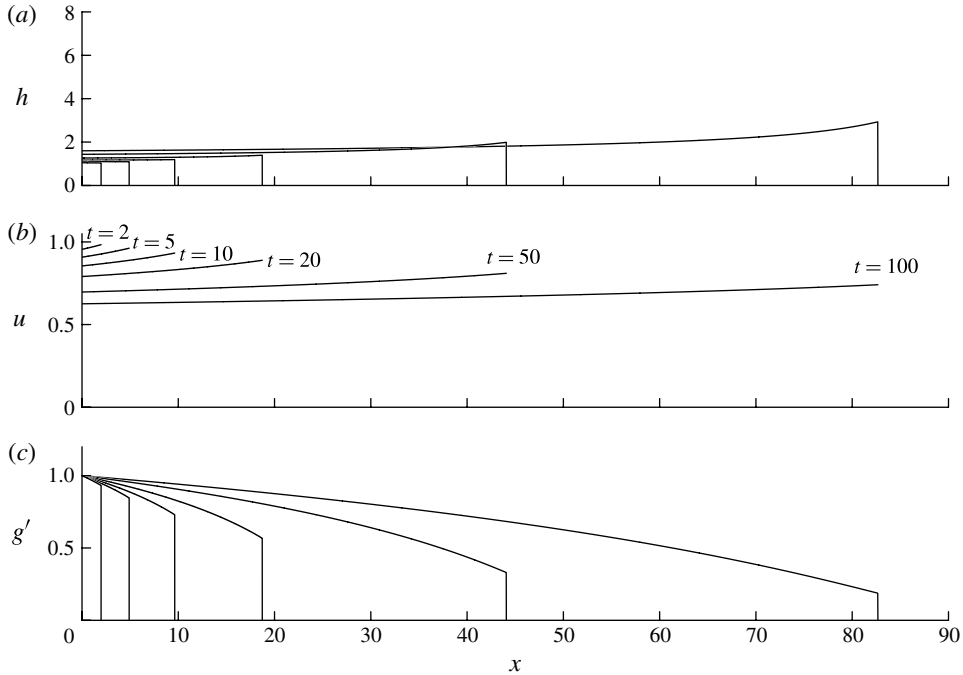
FIGURE 7. The solution at early times of the governing equations of an entraining density current generated by a source of constant flux, (2.13)–(2.15), with $\psi = 27$, $Fr_0 = 1$, $C_D/E_0 = 0$.

solving the inner similarity equations without an entrainment term, does not permit matching of the inner and outer regions. We therefore look for solutions where the entrainment term in (3.3) now balances the other terms, giving an additional equation, $3C - 2A - 2 = 0$, which fully determines the similarity scalings, $\gamma = \alpha = 4/5$, $\beta = -6/5$, $C = 4/5$, $A = 1/5$. Since $C = \gamma$, the inner and outer regions both expand as $t^{4/5}$ and have no scale separation. Thus the inner spatial variables in the inner and outer regions coincide ($\eta = y$), and we expect the transition between the inner and outer regions to occur at $y = y_c$ where $0 < y_c < 1$, with the outer scalings applying in $y_c < y \leqslant 1$ and the inner scalings in $0 \leqslant y < y_c$.

Having determined the scalings, we now seek the form of the similarity solution for a current driven by a sustained buoyancy flux at $x = 0$. Considering the inner region first, substituting the inner scalings into (2.14) implies $(\hat{G}\hat{H}^2)' = 0$, which integrates to give $\hat{G}\hat{H}^2 = K$, a constant. Substituting the inner scalings into (2.13)–(2.15) then gives

$$\frac{2}{5} + 2\hat{U}' = \frac{\hat{U}^3}{\psi K}, \tag{4.1}$$

$$2\left(\hat{U} - \frac{4}{5}\eta\right)\hat{H}' = \frac{\hat{U}^3\hat{H}}{\psi K}. \tag{4.2}$$

Since $\hat{H} \sim t^{1/5}$, whereas in the outer region $H \sim t^{4/5}$, for matching between the two we require $\hat{H}$ to diverge as $y \to y_c$. From (4.2), this is only possible if both $\hat{U} = 4y/5$
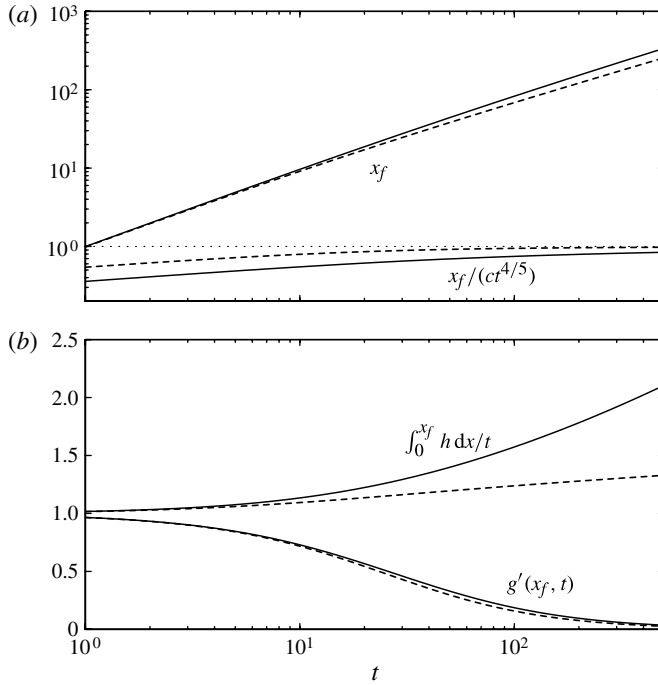
FIGURE 8. The time-evolution of entraining density currents generated by a constant-flux source, determined from time-dependent numerical solutions of the governing equations, with parameters $\psi = 27$, $Fr_0 = 1$ and $C_D/E_0 = 0$ (solid line) and $C_D/E_0 = 0.1$ (dashed line). (a) For both values of C_D/E_0, $x_f \sim ct^{4/5}$ at large times (where c is dependent on C_D/E_0, Fr and ψ); the approach to this long-time behaviour is indicated in the plot of $x_f/(ct^{4/5})$. (b) Reduced gravity at the flow front $g'(x_f, t)$ and the ratio of the total current volume to the volume emitted by the source.

and $\hat{U}' = 4/5$ at $\eta = y_c$ which, from (4.1), implies a relationship between K and y_c,

$$K = \frac{32}{125\psi} y_c^3. \tag{4.3}$$

With the change of variables $\tilde{U} = 5^{4/3}\hat{U}/4y_c$, $\tilde{\eta} = 4y_c\eta/5^{1/3}$, (4.1) reduces to

$$\frac{d\tilde{U}}{d\tilde{\eta}} = \tilde{U}^3 - 1, \tag{4.4}$$

which has the solution

$$\tilde{\eta} = \frac{1}{6}\left[2\ln\left(\tilde{U} - 1\right) - \ln(\tilde{U}^2 + \tilde{U} + 1) - 2\sqrt{3}\tan^{-1}\left(\frac{2\tilde{U} + 1}{\sqrt{3}}\right) \right] + \text{const.} \tag{4.5}$$

However, with the two boundary conditions at $x = 0$ ($c\hat{G} = 1$ and $c^2\hat{H}\hat{U} = 1$), two boundary conditions on U and K at $y = y_c$, and two undetermined parameters, c and y_c, the three similarity equations need one further condition to be determined fully.

This additional condition is found from matching to the outer region, in which the similarity equations are (3.3)–(3.5), with $\gamma = 4/5$. As for the current due to an

instantaneous release, we construct power series for H, U and G about $y = 1$, but now find that a more general series than (3.6) is possible:

$$H = H_0 + H_\lambda s^\lambda + H_1 s + \cdots, \quad U = U_0 + U_1 s + U_\lambda s^{\lambda+1} + \cdots, \\ G = G_0 + G_\lambda s^\lambda + \cdots, \quad \} \tag{4.6}$$

in which non-integer powers of $s = 1 - y$ are present. Substituting into (3.3)–(3.5), with $\gamma = 4/5$, and applying the kinematic condition $U_0 = 4/5$ and the Froude number condition $U_0/(G_0 H_0)^{1/2} = Fr_0$, we find that the all coefficients of integer powers are determined, as is the non-integer power $\lambda = (3/2)(Fr_0^2/(Fr_0^2 + \psi))$. We find also that U_λ and G_λ must be related to H_λ by

$$U_\lambda = \frac{9H_\lambda}{5} \frac{Fr_0^2 + \psi}{5Fr_0^2 + 2\psi}, \quad G_\lambda = -\frac{72H_\lambda}{25Fr_0^6} \left(Fr_0^4 + 2Fr_0^2\psi + \psi^2 \right), \tag{4.7}$$

but that the overall coefficient multiplying the non-integer powers, H_λ, remains undetermined, which introduces one additional unknown into the problem. In the limit $y \to y_c$, we require from matching with the inner solution that $U \to 4y_c/5$ and that $GH^2 \to 32y_c^3/125\psi$.

Solutions to the three outer similarity equations and the two unknown parameters y_c and H_λ are then fully determined by three boundary conditions at $y = 1$ on H, U and G and two conditions at $y = y_c$ on U and GH^2. With y_c determined, the inner solution and the constant c are also then determined. This similarity solution is plotted in figure 9 for a range of ψ. The value of y_c, indicated by the point at which U touches the line $4y/5$, increases with increasing ψ. For $\psi \gtrsim 1$ (including the case $\psi = 27$ inferred from experimental results: see § 3), the outer region $y > y_c$ only occupies a small proportion of the current near $y = 1$; consequently, the concentration g' (denoted by solid lines in figure 9b) remains of the same order as the inflow concentration throughout most of the current. The entrainment in the inner region is small since $Ri \sim t^{3/5}$, whereas in the outer region $Ri = O(1)$ and the bulk of the entrainment occurs. In the experimentally inferred case $\psi = 27$, this restricts the majority of the entrainment to a small region at the current front.

We show the similarity solution for $\psi = 0.1$ in figure 10 with the corresponding numerical solution of (2.13)–(2.15) at $t \approx 2 \times 10^6$. We choose this very late time to illustrate the close matching between the finite-time numerical solution and the long-time similarity solution, which strongly suggests that at late times the similarity solution is realized by time-dependent solutions of the governing equations. In figure 10(b), the same similarity and time-dependent numerical solutions for h are illustrated on a log scale to emphasize the increasing scale separation with time of h (and g') between the inner and outer regions. Whereas the long-time similarity solution (solid lines in figure 10b) predicts that $\hat{H}$ diverges as $y \to y_c$ from below and that $H \to 0$ as $y \to y_c$ from above, at the finite time illustrated in this solution, the time-dependent numerical solution (dashed line) instead exhibits a transition region when $y \approx y_c$ between the inner and outer scalings for h.

4.1. *Constant entrainment coefficient*

When the entrainment coefficient is constant ($\psi = 0$), as used by Ross *et al.* (2006), we find that gravity currents driven by a sustained flux at the source evolve in a different manner from those governed by the variable entrainment coefficient described above. This behaviour is analogous to the lock-release currents with constant entrainment coefficient, described in § 3.2, and we approach the problem as before,
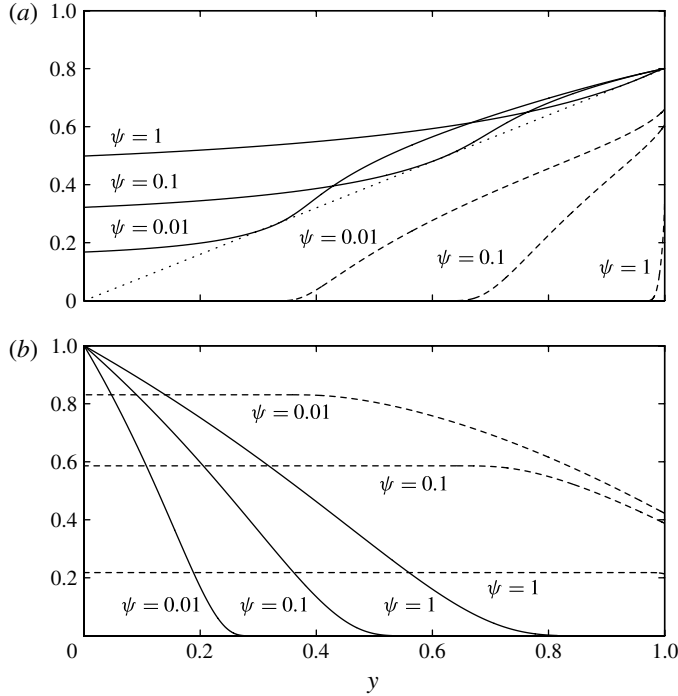
FIGURE 9. Long-time similarity solutions for a current generated by a source of constant flux, for $Fr_0 = 1$, across a range of values of ψ. In (*a*), dashed lines represent H in the outer region and solid lines represent U. The dotted line is $4y/5$. In (*b*), dashed lines represent GH^2 and solid lines g' in the inner solution.

looking first for solutions with 'inner' and 'outer' regions that obey the scalings (3.1) and (3.2). It can be shown that the entrainment flux $E|u|$ must balance the other terms in the mass equation, which implies that $C = A = 1/2$ and $\gamma = 1$. Thus in the outer region we have $x \sim t$, $h \sim t$, $u \sim 1$ and $g' \sim t^{-1}$, while in the inner we have $x \sim t^{1/2}$, $h \sim t^{1/2}$, $u \sim t^{-1/2}$ and $g' \sim 1$. Notably, each region then contributes to the overall buoyancy ($g'hx$) with the same linear time dependence.

With these scalings, the similarity equations in the outer region become

$$H - yH' + (HU)' = U, \tag{4.8}$$

$$-yU' + UU' + GH' + \frac{1}{2}HG' = -\frac{U^2}{H}, \tag{4.9}$$

$$-G - yG' + UG' = -\frac{UG}{H}, \tag{4.10}$$

with the source condition $UGH = 1/c^3$ at $y = 0$ and front conditions $U = 1$ and $U = Fr_0\sqrt{GH}$ (which becomes $GH = Fr_0^2$) at $y = 1$. These outer equations cannot be solved analytically, but by carefully expanding the dependent variables close to the origin (details in appendix C), we find that

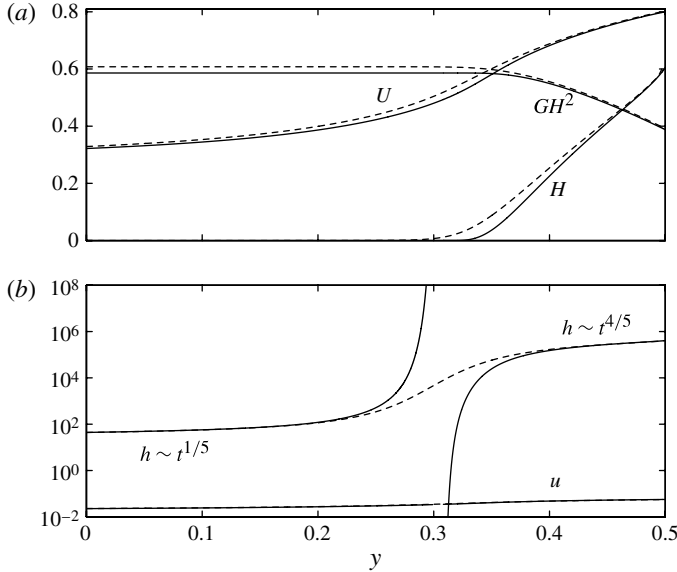$$H = \frac{y}{2} + \frac{y}{4\log(k_1/y)} + \cdots, \tag{4.11}$$

FIGURE 10. The similarity solution and the time-dependent numerical solution at $t = 2 \times 10^6$ for a current generated by a source of constant flux with $\psi = 0.1$. Solid lines indicate the similarity solution; dotted lines indicate the time-dependent solution. In (*a*), the solution is scaled to the outer similarity scalings; in (*b*), a log scale on the vertical axis illustrates the separation of scales between the inner and outer regions.

$$U = y \log (k_1/y) + \cdots, \qquad (4.12)$$

$$GH^2 = k_2 + \cdots, \qquad (4.13)$$

where k_1 and k_2 are constants. This analysis reveals two features that together mean that a straightforward similarity solution is not applicable. First, the reduced gravity $G \sim 4k_2/y^2$ when $y \ll 1$, and thus requires an inner region of size $y \sim t^{-1/2}$ to match the boundary condition $g' = 1$. Second, the buoyancy flux at the origin, $UGH = 2k_2 \log(k_1/y)$ when $y \ll 1$, diverges logarithmically as the source is approached, suggesting that logarithmic corrections to the scalings will be required. Both of these features are analogous to a current generated by an instantaneous release of dense fluid (§ 3.2).

On this basis, we introduce variables in the outer region of the form

$$h = x_f \tilde{H}(y, t), \quad u = \dot{x}_f \tilde{U}(y, t) \quad \text{and} \quad g = \frac{\dot{x}_f^2}{x_f} \tilde{G}(y, t), \qquad (4.14)$$

where $x_f = t\xi(t)$. At long times ($t \gg 1$), we seek solutions of the form

$$\tilde{H}(y, t) = \tilde{H}_0(y) + \cdots, \quad \tilde{U}(y, t) = \tilde{U}_0(y) + \cdots \quad \text{and} \quad \tilde{G}(y, t) = \tilde{G}_0(y) + \cdots, \quad (4.15)$$

and assume that $t \, d\xi/dt \ll \xi$. Substituting these into the governing equations, we obtain expressions for $\tilde{H}_0$, $\tilde{U}_0$ and $\tilde{G}_0$ that are identical to solutions of (4.8)–(4.10). In particular, these show that this leading-order expression for the reduced gravity becomes comparable with the source condition when $y \sim \delta = \dot{x}_f/x_f^{1/2}$.

Within the inner region, we therefore adopt the spatial coordinate $Y = y/\delta$ and construct the following leading-order expansions for the dependent variables:

$$h = \left(\dot{x}_f^2 x_f\right)^{1/2} \bar{H}_0(Y) + \cdots, \quad u = \left(\dot{x}_f^3 x_f^{-1}\right)^{1/2} \bar{U}_0(Y) + \cdots, \quad g' = \bar{G}_0(Y) + \cdots. \quad (4.16)$$

This implies that to leading order, the governing equations are then given by

$$\frac{\bar{H}_0}{2} - \frac{Y}{2}\bar{H}_0' + (\bar{H}_0\bar{U}_0)' = \bar{U}_0, \quad (4.17)$$

$$\bar{G}_0\bar{H}_0 - \frac{1}{2}\left(Y\bar{G}_0\bar{H}_0\right)' + \left(\bar{U}_0\bar{G}_0\bar{H}_0\right)' = 0, \quad (4.18)$$

$$\left(\bar{G}_0\bar{H}_0^2\right)' = 0, \quad (4.19)$$

to which we add the source conditions $\bar{U}_0\bar{H}_0\bar{G}_0 = \dot{x}_f^{-5/2}$ and $\bar{G}_0 = 1$ at $Y = 0$. Immediately, we note that we can match to the outer region to determine

$$\bar{G}_0\bar{H}_0^2 = k_2. \quad (4.20)$$

To complete the solution, we need to apply the boundary conditions at the source, which is most easily accomplished by integrating (4.18) over the inner boundary layer. This yields

$$\int_0^{\delta^\mu} \bar{G}_0\bar{H}_0 \, dY + \left[\left(U - \frac{Y}{2}\right)\bar{G}_0\bar{H}_0\right]_0^{\delta^\mu} = 0, \quad (4.21)$$

where μ is a constant ($\mu < 0$), and we anticipate that the leading-order matching will be independent of μ. From matching the two asymptotic regions, we have $\bar{U}_0\bar{H}_0\bar{G}_0 = \dot{x}_f^{1/2}2k_2\log(k_3/\delta^{\mu+1})$ (where k_3 is a constant) and we evaluate the first term of (4.21) to leading order by using (4.20) in a manner analogous to §3.2, to find that

$$2k_2\log(\delta^\mu) + 2k_2\log\frac{k_3}{\delta^{\mu+1}} - \frac{1}{\dot{x}_f^3} = 0. \quad (4.22)$$

Substituting the leading-order expression for δ, we find that

$$x_f(t) \sim \frac{t}{(k_2 \log t)^{1/3}}. \quad (4.23)$$

The constant k_2 can be determined by solution of the boundary value problem (4.8)–(4.10), illustrated in figure 12. As before, a power series of the form (4.6) at $y = 1$ determines three boundary conditions, but introduces one undetermined coefficient multiplying the non-integer powers of s (we now have $\lambda = 1/2$). The boundary condition $U \to 0$ as $y \to 0$ closes the system, and by a shooting method we find $k_2 = 2.19\ldots$ for $Fr_0 = 1$, $C_D = 0$.

The similarity between the long-time asymptotic growth rate (4.23) and current length x_f found from numerical solution of the governing equations is illustrated in figure 11.

5. Summary and conclusions

We have studied a model for gravity currents that combines depth-integrated conservation equations for the current with an empirically determined model of fluid entrainment that is parameterized by the bulk Richardson number. We have calculated long-time similarity solutions of this model, corresponding to a current driven by
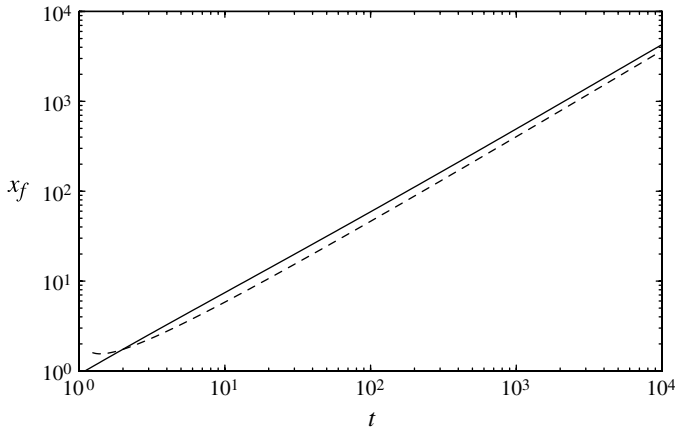
FIGURE 11. The dimensionless front position x_f as a function of time for an entraining density current generated by a source of constant flux, with a constant entrainment coefficient ($\psi = 0$), determined from time-dependent numerical solutions of the governing equations (solid line). The long-time asymptotic solution given by (4.23) is indicated by a dashed line.
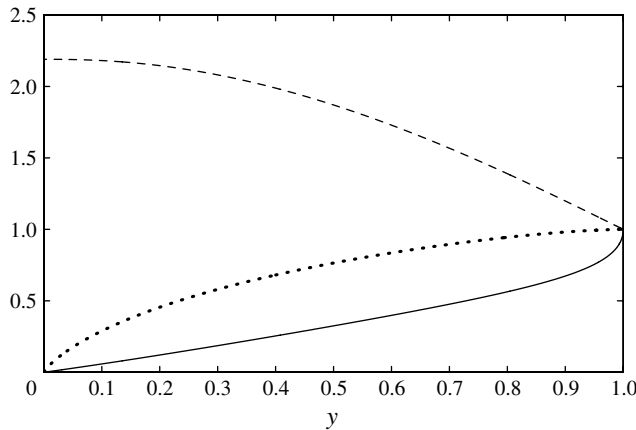

FIGURE 12. Solution of the outer similarity equations in the case of a constant entrainment coefficient and constant buoyancy flux. The solid line indicates H, the dotted line U and the dashed line GH^2.

either an instantaneous release, or by a constant flux, of dense fluid. In both cases, we find that the effects of mixing are most significant close to the front of the current, where its motion is retarded and its depth increased. Close to the rear, in contrast, exhibits relatively little entrainment. This leads to a two-region structure, in which scalings close to the back of the current differ from those near the front. In currents caused by an instantaneous release, the long-time solution is a similarity solution of the second kind, with current length scaling as t^γ, where γ is a weak function of the entrainment parameterization; in particular, if $E = E_0/(1 + \psi Ri)$, the exponent depends on ψ. With $Fr_0 = 1$ and $C_D/E_0 = 0$, for $\psi = 27$, the value determined by the experimental data, we find that $x_f \sim t^{0.447}$. In currents caused by a constant flux of buoyancy, the length of the similarity solution scales as $t^{4/5}$. Both of these solutions

are distinct, in solution structure and in growth rate, from the solutions obtained if entrainment is either neglected or is considered to be independent of the Richardson number.

In the non-entraining buoyancy-inertial regime, the Froude number condition at the current front, together with the global buoyancy (2.7) or (2.9), are sufficient to construct a 'box model' that captures the temporal evolution of the flow (Dade & Huppert 1995). In these non-entraining currents, the frontal Froude number condition plays a crucial role in determining the flow evolution, which is one reason why box models have been successful. In the entraining regime, however, the front exerts a much weaker role on the overall structure of the flow in entraining currents than it does in non-entraining currents, leading to only relatively minor variations in the exponent of the spreading rate (figure 5*a*). The scalings in the outer region, where the frontal Froude number is applied, are different from those in the inner region, where the dominant contribution to the total buoyancy originates, precluding the use of a conventional box model. The existence of a similarity solution of the second kind for entraining 'lock-release' currents, and the consequent determination of current scalings through an eigenvalue problem, is additional evidence that simple box models or dimensional arguments are insufficient to calculate the scalings in the entraining regime.

Our addition of entrainment to shallow water gravity current models is motivated by the observation that, for currents in the buoyancy-inertia similarity regime, the effect of entrainment becomes increasingly important over time. In currents caused by a release of a finite volume of dense fluid, we therefore predict a transition from the buoyancy-inertia regime (Hoult 1972) to a new entraining regime in which $x_f \sim t^{0.447}$. Rottman & Simpson (1983) present results from laboratory experiments (their figure 12) which show three distinct phases of gravity current propagation: an initial adjustment phase where $x_f \sim t$, followed by a buoyancy-inertia phase where $x_f \sim t^{2/3}$, followed by a viscous self-similar phase where $x_f \sim t^{1/5}$. From the results obtained in this paper, we propose the existence of a fourth regime, between the buoyancy-inertia and viscous self-similar phases, in which entrainment is important and $x_f \sim t^{0.447}$, which is only attained if the current is large enough for the onset of viscous forces to occur later than the onset of entrainment.

A consequence of the relatively late onset of entrainment effects is that observations of the flow structures that we describe may be difficult to obtain in laboratory experiments, especially given the care required to obtain quantitative experimental measurements of the entrainment rate. Nevertheless, with verification of our results in mind, we describe in appendix A how depth-averaged variables h, u and g' relate to the three-dimensional velocity and concentration fields that may be obtained from experimental measurements or fully three-dimensional numerical simulations.

The 'head' of a gravity current has long been recognized as an important component of the flow, both in influencing flow dynamics through a constant Froude number condition, and as a region in which the majority of fluid entrainment occurs. Rather than specifying in our model that entrainment occurs only near the flow front, we have taken the approach of applying a single model (2.13)–(2.15) throughout the entire current. We find that a region near the flow front, with properties distinct from the bulk of the current and consistent with experimental observations of gravity current heads, emerges in the solution of this model. In particular, at late times and for realistic values of ψ, the Richardson number is of order unity only near the front of the current, in both currents caused by a constant flux and in those caused by an instantaneous release. The entrainment coefficient is therefore close to its

maximum value only near to the current front, a feature in agreement with laboratory experiments (Hallworth *et al.* 1996).

Finally, we remark that the results from this study reinforce the need for experiments at sufficiently large scale to reveal the effects of entrainment on the propagation of gravity currents. Our results are built upon a simple, but widely used, model of entrainment. Implicitly assumed is that the density of fluid within the current remains vertically well mixed, and this requires sufficiently vigorous turbulent fluctuations. As the magnitude of the turbulence wanes, we anticipate that an internal stratification develops within the gravity current and this requires a new class of model to capture the developing features. Some aspects of this effect are reproduced in the multi-layer models of Arita & Jirka (1987), Sorgard (1991) and Hogg, Hallworth & Huppert (2005), although these were developed for situations with a co- or counter-flowing ambient. Nevertheless, they offer some interesting insights and may be valuable for future developments of models of entraining gravity currents.

Acknowledgement

Appendix A. Derivation of the depth-integrated model

For gravity currents driven by density differences due to a dissolved solute, the mean solute concentration $c^\star$ (averaged over turbulent fluctuations) is governed by the equation

$$\frac{\partial c^\star}{\partial t} + (\boldsymbol{u}^\star \cdot \nabla)c^\star = \nabla \cdot \boldsymbol{F}, \tag{A 1}$$

where $\boldsymbol{u}^\star = (u^\star, w^\star)$ is the mean flow velocity and $\boldsymbol{F}$ represents the flux of solute due to turbulent fluctuations (we assume that the Péclet number is large enough for all mixing at the scale of the current to be due to turbulence). Assuming that variations in the mean flow variables occur on much longer horizontal length scales than vertical ones, and therefore that the horizontal component of the Reynolds flux is much smaller than the vertical, reduces (A 1) to

$$\frac{\partial c^\star}{\partial t} + (\boldsymbol{u}^\star \cdot \nabla)c^\star = \frac{\partial F}{\partial z}, \tag{A 2}$$

where F is the z-component of $\boldsymbol{F}$. We introduce the function $h(x, t)$, where $z = h$ will represent the surface of the flow. Considering h for now to be an arbitrary positive function, integrating from $z = 0$ to $z = h$ and applying the boundary condition of no flux through the base of the flow $z = 0$ gives

$$\frac{\partial}{\partial t}\left[\int_0^h c^\star \, \mathrm{d}z\right] + \frac{\partial}{\partial x}\left[\int_0^h u^\star c^\star \, \mathrm{d}z\right] = \left\{c^\star\left(\frac{\partial h}{\partial t} + u^\star \frac{\partial h}{\partial x} - w^\star\right) + F\right\}_{z=h}. \tag{A 3}$$

Integrating the equation for conservation of mass for incompressible flow, $\nabla \cdot \boldsymbol{u}^\star = 0$, gives

$$\frac{\partial}{\partial x}\left[\int_0^h u^\star \, \mathrm{d}z\right] + \left\{-u^\star \frac{\partial h}{\partial x} + w^\star\right\}_{z=h} = 0, \tag{A 4}$$

which simplifies (A 3) to

$$\frac{\partial}{\partial t} \left[\int_0^h c^\star \, \mathrm{d}z \right] + \frac{\partial}{\partial x} \left[\int_0^h u^\star c^\star \, \mathrm{d}z \right] = c^\star \left\{ \frac{\partial h}{\partial t} + \frac{\partial}{\partial x} \left[\int_0^h u^\star \, \mathrm{d}z \right] + \frac{F}{c^\star} \right\}_{z=h}, \quad \text{(A 5)}$$

where, physically, the right-hand side represents the mean flux of solute through the interface $z = h(x, t)$. We now specify that, since h represents the surface of the current, this flux is zero, resulting in the two constraints on h:

$$\frac{\partial h}{\partial t} + \frac{\partial}{\partial x} \left[\int_0^h u^\star \, \mathrm{d}z \right] = -\left(\frac{F}{c^\star} \right)_{z=h}, \quad \text{(A 6)}$$

$$\frac{\partial}{\partial t} \left[\int_0^h c^\star \, \mathrm{d}z \right] + \frac{\partial}{\partial x} \left[\int_0^h u^\star c^\star \, \mathrm{d}z \right] = 0. \quad \text{(A 7)}$$

The equation for conservation of mean fluid momentum is

$$\rho \left(\frac{\partial \boldsymbol{u}^\star}{\partial t} + (\boldsymbol{u}^\star \cdot \boldsymbol{\nabla}) \boldsymbol{u}^\star \right) + \boldsymbol{\nabla} p - \rho \boldsymbol{g} = \boldsymbol{\nabla} \cdot (\rho \boldsymbol{R}), \quad \text{(A 8)}$$

where $\boldsymbol{g} = (0, g)$ is the gravity vector and the tensor $\rho \boldsymbol{R}$ is the momentum flux due to turbulent fluctuations; we assume that the Reynolds number is sufficiently large for the molecular viscosity to be negligible. The fluid pressure is denoted by p and the fluid density by ρ, which are related to solute concentration through

$$\rho(x, z, t) = \rho_0 + \rho_1 c^\star(x, z, t). \quad \text{(A 9)}$$

Supposing as before that the horizontal length scale of the flow is much greater than the vertical, and also that the density differences due to solute concentration are small, i.e. $c \rho_1 \ll \rho_0$, the horizontal and vertical components of (A 8) simplify to

$$\frac{\partial u^\star}{\partial t} + \left(u^\star \frac{\partial}{\partial x} + w^\star \frac{\partial}{\partial z} \right) u^\star = -\frac{1}{\rho_0} \frac{\partial \tilde{p}}{\partial x} + \frac{\partial R}{\partial z}, \quad \text{(A 10)}$$

$$0 = -\frac{1}{\rho_0} \frac{\partial \tilde{p}}{\partial z} + \frac{\rho_1 c^\star}{\rho_0} g, \quad \text{(A 11)}$$

where $R = R_{xz}$ and $\tilde{p} = p + \rho_0 g z$. Integrating (A 11) with the boundary condition that the p tends to its ambient hydrostatic value $-\rho g z$ as $z \to \infty$ gives

$$\tilde{p} = \rho_1 g \int_z^\infty c^\star \, \mathrm{d}z. \quad \text{(A 12)}$$

Integrating (A 10) in z, and using (A 6) then gives

$$\frac{\partial}{\partial t} \left[\int_0^h u^\star \, \mathrm{d}z \right] + \frac{\partial}{\partial x} \left[\int_0^h u^{\star 2} \, \mathrm{d}z + \frac{g \rho_1}{\rho_0} \int_0^h \int_z^\infty c^\star \, \mathrm{d}z' \mathrm{d}z \right] = \left[\left(\frac{R}{u^\star} - \frac{F}{c^\star} \right) u^\star \right]_{z=0}^{z=h}. \quad \text{(A 13)}$$

We now suppose that c and u take the similarity form

$$c^\star(x, z, t) = c(x, t) C(\eta), \quad u^\star(x, z, t) = u(x, t) U(\eta), \quad \text{(A 14)}$$

where $\eta = z/h(t)$ and C and U are functions that represent the vertical structure of the current. Without loss of generality, we specify that $\int_0^1 C \, \mathrm{d}\eta = \int_0^1 U \, \mathrm{d}\eta = 1$, which reduces (A 6), (A 7) and (A 13) to

$$\frac{\partial h}{\partial t} + \frac{\partial}{\partial x} (hu) = w_e, \quad \text{(A 15)}$$

$$\frac{\partial}{\partial t}\left(hg'\right) + k_{uc}\frac{\partial}{\partial x}\left(hug'\right) = 0, \tag{A 16}$$

$$\frac{\partial}{\partial t}\left(hu\right) + k_{uu}\frac{\partial}{\partial x}\left(hu^2\right) + (k_{c_1} + k_{c_2})\frac{\partial}{\partial x}\left(\frac{g'h^2}{2}\right) = \left[\left(\frac{R}{u^\star} - \frac{F}{c^\star}\right)u^\star\right]_{z=0}^{z=h}, \tag{A 17}$$

where $w_e = F/c^\star_{z=h}$, the reduced gravity, g', is defined by $g' = g\rho_1 c/\rho_0$, and the shape factors

$$k_{uu} = \int_0^1 U^2\,\mathrm{d}\eta, \quad k_{uc} = \int_0^1 UC\,\mathrm{d}\eta, \quad k_{c_1} = 2\int_0^1 \eta C\,\mathrm{d}\eta, \quad k_{c_2} = 2\int_1^\infty C\,\mathrm{d}\eta \tag{A 18}$$

are constants. We select h so that a negligible proportion of the buoyancy lies above $h = 1$, which implies $k_{c_2} \ll k_{c_1}$. The value of the shape factors may play a significant role in determining the behaviour near a current front in which $h \to 0$ (Hogg & Pritchard 2004). However, for simplicity we set the shape factors k_{uc}, k_{c_1} and k_{uu} to unity, an assumption supported by measurements of experimental turbidity currents (Parker *et al.* 1986). If the Schmidt number (or Prandtl number, for currents driven by temperature-induced density differences), is unity, the Reynolds fluxes for concentration F and velocity R are equal, when normalized with respect to the concentration and velocity that they respectively transport, and the source term on the right-hand side of (A 17) is zero. If the Schmidt or Prandtl number is not unity, by analogy with the entrainment hypothesis (Turner 1986) we take the relevant velocity scale in the fluxes R and F to be u, and thus obtain a right-hand side for (A 17) of the form $-C_D u|u|$, where C_D is assumed to be a constant. This term represents drag caused by effects other than the entrainment of quiescent ambient fluid, in particular basal drag.

Appendix B. Early-time effects of entrainment on non-entraining similarity solutions

In this appendix, we analyse the early-time deviations of the motion of an entraining gravity current from the non-entraining similarity solutions that capture the motion governed by a balance between fluid inertia and buoyancy. In terms of the dimensionless variables introduced in §2, these expression are formally valid when $t \ll 1$, with appreciable entrainment occurring on a time scale $t = O(1)$. Our methods here for deriving these deviations from the leading-order solutions follow closely those developed in the context of particle-driven currents (Hogg, Ungarish & Huppert 2000; Harris, Hogg & Huppert 2001) or drag-affected flows (Hogg & Woods 2001).

B.1. *Currents with constant buoyancy*

The similarity solution in the absence of entrainment during the inertia-buoyancy phase of the motion was given by Hoult (1972):

$$h = h_0(x, t) = t^{-2/3}H_0(y_0) = \frac{K^2}{9t^{2/3}}\left(y_0^2 - 1 + \frac{4}{Fr_0^2}\right), \tag{B 1}$$

$$u = u_0(x, t) = t^{-1/3}KU_0(y_0) = \frac{2Ky_0}{3t^{1/3}}, \tag{B 2}$$

$$x_f = x_{f0}(t) = Kt^{2/3}, \tag{B 3}$$

where $y_0 = x/x_{f0}$ and $K = (27Fr_0^2/(12 - 2Fr_0^2))^{1/3}$. This similarity solution represents the asymptotic solution of the motion from lock-release and other initial conditions

(see, e.g., Hogg 2006; Mathunjwa & Hogg 2006). We seek the perturbation to this solution due to the effects of entrainment. It was identified in §2 that entrainment effects are no longer negligible and begin to influence the motion when $t^{4/3} = O(1)$ in terms of the dimensionless variables. We deduce, therefore, that the perturbation to the inertia-buoyancy similarity solution (B 1)–(B 3) is proportional to $t^{4/3}$ and accordingly write

$$h = t^{-2/3} H_0(y_0) + t^{2/3} H_1(y_0) + \cdots, \quad u = K \left(t^{-1/3} U_0(y_0) + t U_1(y_0) + \cdots \right), \quad \text{(B 4)}$$

$$g' = 1 + t^{4/3} G_1(y_0) + \cdots, \quad x_f = x_{f0}(t) + K X_1 t^2 + \cdots, \quad \text{(B 5)}$$

where the perturbation functions $H_1(y_0)$, $U_1(y_0)$, $G_1(y_0)$ and the constant X_1 are to be determined. Substituting these expansions into the governing equations (2.14)–(2.15) and balancing terms in equal powers of t in the regime $t \ll 1$ leads to

$$\frac{4}{3} H_1 + (H_0 U_1)' = \frac{K U_0}{1 + \psi R i_0}, \quad \text{(B 6)}$$

$$\frac{5}{3} U_1 + \frac{1}{K^2} \left(H_1' + G_1 H_0' + \frac{1}{2} H_0 G_1' \right) = -\frac{K U_0^2}{H_0} \left(\frac{1}{1 + \psi R i_0} + \frac{C_D}{E_0} \right), \quad \text{(B 7)}$$

$$G_1 = -\frac{K U_0}{H_0} \frac{1}{1 + \psi R i_0}, \quad \text{(B 8)}$$

where $R i_0 = H_0 / (K U_0)^2$. These linearized equations governing the perturbation to the similarity solution must be supplemented by boundary conditions. First, we enforce no flow at the rear boundary $x = 0$, which implies that $U_1(0) = 0$. At the front of the current, we require for kinematic consistency that $U_1(1) = (4/3) X_1$, and the dynamic condition (2.10) then implies that

$$4 K^2 G_1(1) + 9 Fr_0^2 H_1(1) + \left(\tfrac{8}{3} Fr_0^2 - 32 \right) K^2 U_1(1) = 0. \quad \text{(B 9)}$$

This system (B 6)–(B 8) and associated conditions is therefore a boundary value problem for $H_1(y_0)$ and $U_1(y_0)$, which may be readily solved numerically. We plot the solution for $\psi = 27$, $Fr_0 = 1$, $C_D/E_0 = 0$, and $\psi = 27$, $Fr_0 = 1$, $C_D/E_0 = 0.1$ in figure 13(a). Two universal effects of entrainment at early times, brought out through these perturbations, are that the reduced gravity is diminished and the motion is slowed. The reduction in density difference between the current and the surroundings is largest close to the front; this arises because the Richardson number of the flow monotonically decreases along the length of the current, reaching a minimum value at the front, where the mixing is maximized. The flow height is increased along the entire current when $C_D/E_0 = 0$, reflecting the increase in current volume due to entrainment, but for sufficiently large basal drag, including the case $C_D/E_0 = 0.1$, a region close to the front is reduced in height as the current develops a streamwise pressure gradient to sustain its motion. The perturbation to the front position $X_1 = -0.00204$ for $C_D/E_0 = 0$ and $X_1 = -0.00642$ for $C_D/E_0 = 0.1$. This indicates that the expansion of x_f (B 5) becomes non-asymptotic at $t \approx 100$ (for $C_D/E_0 = 0$) or $t \approx 30$ (for $C_D/E_0 = 0.1$), reflecting the validity of this expansion at early times only.

B.2. *Currents due to a constant buoyancy flux*

The similarity solutions for a current generated by a constant-flux source of buoyancy in the absence of entrainment and during the inertia-buoyancy phase of the motion were given by Gratton & Vigo (1994), and depend on the Froude numbers at the front
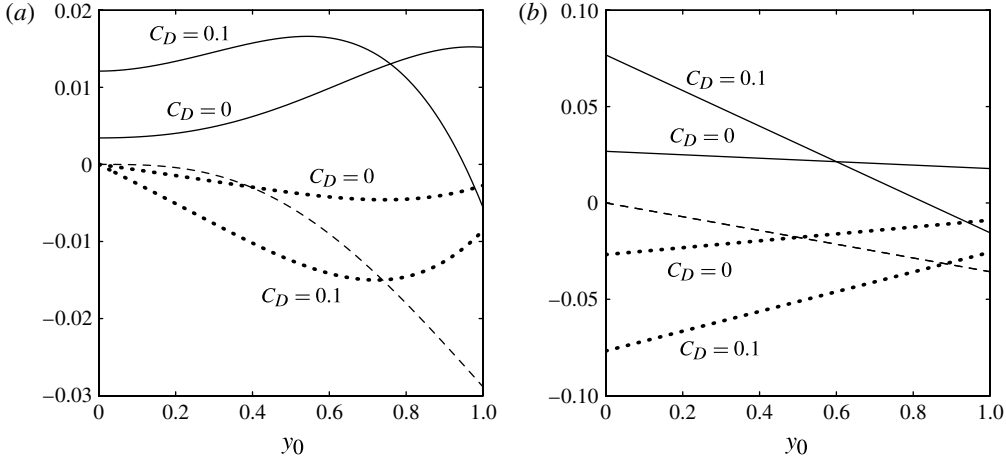
FIGURE 13. The form of the early-time perturbations to the non-entraining similarity solution resulting from entrainment and drag, showing $H_1(y_0)$ (solid line), $U_1(y_0)$ (dotted line) and $G_1(y_0)$ (dashed line), for $\psi = 27$, $Fr_0 = 1$, and $C_D/E_0 = 0$ and 0.1 In (a), the perturbations for a constant total buoyancy are shown; in (b), the perturbations are to the similarity solution with a constant buoyancy flux.

and the back of the current. The simplest situation is that these are equal, and the velocity and height fields are both constant:

$$h = h_0(x, t) = Fr_0^{-2/3}, \quad u = u_0(x, t) = Fr_0^{2/3} \quad \text{and} \quad x_f = x_{f0}(t) = Fr_0^{2/3}t. \quad \text{(B 10)}$$

In terms of this solution, the Richardson number is constant $Ri_0 = Fr_0^{-2}$. We now seek perturbations to this solution due to the effects of entrainment, which in terms of the dimensionless variables occurs when $t = O(1)$. Thus we seek the form of the perturbation by writing

$$h = Fr_0^{-2/3} + tH_1(y_0) + \cdots, \quad u = Fr_0^{2/3} + tU_1(y_0) + \cdots, \quad \text{(B 11)}$$

$$g' = 1 + tG_1(y_0) + \cdots, \quad x_f = Fr_0^{2/3}t + X_1t^2 + \cdots, \quad \text{(B 12)}$$

where the perturbation functions $H_1(y_0)$, $U_1(y_0)$, $G_1(y_0)$ and the constant X_1 are to be determined. Substituting these expansions into the governing equations (2.14)–(2.15) and balancing terms in equal powers of t in the regime $t \ll 1$ leads to

$$Fr_0^{-4/3}U_1' + (1 - y_0)H_1' = \frac{Fr_0^{2/3}}{1 + \psi Ri_0} - H_1, \quad \text{(B 13)}$$

$$(1 - y_0)U_1' + Fr_0^{-2/3}H_1' + \frac{1}{2}Fr_0^{-4/3}G_1' = -\frac{C_D}{E_0}Fr_0^2 - \frac{Fr_0^2}{1 + \psi Ri_0} - U_1, \quad \text{(B 14)}$$

$$(1 - y_0)G_1 = -\frac{Fr_0^2}{1 + \psi Ri_0} - G_1. \quad \text{(B 15)}$$

This system is solved subject to the following boundary conditions. First, the reduced gravity at the source is imposed and so the perturbation must vanish: $G_1(0) = 0$. The buoyancy flux is imposed at source, which implies that

$$Fr_0^{2/3}H_1(0) + Fr_0^{-2/3}U_1(0) = 0. \quad \text{(B 16)}$$

At the front, the kinematic condition implies $2X_1 = U_1(1)$ and the Froude number condition leads to

$$2Fr_0^{2/3}U_1(1) = Fr_0^2\left(Fr_0^{-2/3}G_1(1) + H_1(1)\right). \tag{B 17}$$

This system is readily integrated to find the perturbation functions and the value X_1. In fact, it is straightforward to show that H_1, U_1 and G_1 are linear functions of y_0, and for the case $Fr_0 = 1$ we find

$$H_1 = -\left(\frac{5C_D}{6E_0} + \frac{1}{4(1+\psi)}\right)y + \frac{C_D}{2E_0} + \frac{3}{4(1+\psi)}, \tag{B 18}$$

$$U_1 = \left(\frac{C_D}{3E_0} + \frac{1}{2(1+\psi)}\right)y - \frac{C_D}{2E_0} - \frac{3}{4(1+\psi)}, \tag{B 19}$$

$$G_1 = -\frac{y}{1+\psi} \tag{B 20}$$

and $X_1 = -C_D/[12E_0] - 1/[8(1+\psi)]$.

These profiles are plotted in figure 13(b), again for $\psi = 27$, $C_D/E_0 = 0$ and $C_D/E_0 = 0.1$. As with the perturbations to similarity solutions with constant buoyancy, the current velocity and reduced gravity are decreased along the length of the current (with the greatest dilution occurring at the front) and the current height is increased everywhere for sufficiently small values of C_D/E_0 but decreased near the current front for larger C_D/E_0. These perturbations bring out many of the features of numerical time-dependent solution (figure 7) at very early times. As with the perturbations to currents generated by an instantaneous release of dense fluids, the size of the perturbation to the current front position, $X_1 = -0.00700$ for $C_D/E_0 = 0$ and $X_1 = -0.0192$ for $C_D/E_0 = 0.1$, means that the expansion of x_f (B 12) becomes non-asymptotic at $t \approx 30$. This is evident in the numerical solutions of the time-dependent equations (figure 7), where for $t \gtrsim 20$ features of the entraining similarity solution not present in the early-time perturbation, such as the peak in h at the front, become increasingly evident.

Appendix C. Currents generated by a continuous source with constant entrainment ($\psi = 0$): outer solution in the region $y \ll 1$

Rearranging (4.10) in terms of H and GH^2, and neglecting derivatives of GH^2 (since we suspect that $GH^2 \to K$, a constant, as $y \to 0$),

$$(U - y)H' = \tfrac{1}{2}(U - H) \tag{C 1}$$

and (4.8) then becomes

$$HU' = U - H - (U - y)H' = \tfrac{1}{2}(U - H). \tag{C 2}$$

Defining $V = U/y$ and $\Theta = H/y - 1/2$, these give

$$\frac{dV}{d\Theta} = \frac{(V-1)\left(-V\Theta - \dfrac{1}{4} - \dfrac{\Theta}{2}\right)}{\left(V + \dfrac{1}{2}\right)\left(-V\Theta + \dfrac{1}{4} + \dfrac{\Theta}{2}\right)}, \tag{C 3}$$

from which we obtain

$$V = \frac{1}{4\Theta} - \frac{1}{2} + 8\Theta + \cdots. \tag{C 4}$$

Equation (C 1) then becomes the separable ODE

$$y\Theta' = \frac{-V\Theta + \dfrac{1}{4} + \dfrac{\Theta}{2}}{V - 1} = 4\Theta^2 - 8\Theta^3 + \cdots, \tag{C 5}$$

which, integrating and rearranging for Θ, gives

$$\Theta = -\frac{1}{4\log(k_1/y)} + \cdots, \tag{C 6}$$

where k_1 is the constant of integration. Substituting for H and V, (C 4) and (C 6) give the result (4.11)–(4.13).

REFERENCES

ARITA, M. & JIRKA, G. H. 1987 Two-layer model of saline wedge I: entrainment and interfacial friction. *J. Hydraul. Engng* **113**, 1229–1247.

BAINES, P. G. 2001 Mixing in flows down gentle slopes into stratified environments. *J. Fluid Mech.* **443**, 237–270.

BARENBLATT, G. I. 1996 *Scaling, Self-similarity, and Intermediate Asymptotics*. Cambridge University Press.

BENJAMIN, T. B. 1968 Gravity currents and related phenomena. *J. Fluid Mech.* **31**, 209–248.

BONNECAZE, R. T. & LISTER, J. R. 1999 Particle-driven gravity currents down planar slopes. *J. Fluid Mech.* **390**, 75–91.

BRITTER, R. E. & LINDEN, P. F. 1980 The motion of the front of a gravity current travelling down an incline. *J. Fluid Mech.* **99**, 531–543.

BRITTER, R. E. & SIMPSON, J. E. 1978 Experiments on the dynamics of a gravity current head. *J. Fluid Mech.* **88**, 223–240.

CHRISTODOULOU, G. C. 1986 Interfacial mixing in stratified flows. *J. Hydraul Res.* **24** (2), 77–92.

DADE, W. B. & HUPPERT, H. E. 1995 A box model for non-entraining, suspension-driven gravity surges on horizontal surfaces. *Sedimentology* **42** (3), 453–470.

ELLISON, T. H. & TURNER, J. S. 1959 Turbulent entrainment in stratified flows. *J. Fluid Mech.* **6**, 423–448.

FERNANDEZ, R. L. & IMBERGER, J. 2006 Bed roughness induced entrainment in a high Richardson number underflow. *J. Hydraul Res.* **44** (6), 725–738.

FERNANDO, H. J. S. 1991 Turbulent mixing in stratified fluids. *Annu. Rev. Fluid Mech.* **23**, 455–493.

GRATTON, J. & VIGO, C. 1994 Self-similar gravity currents with variable inflow revisited: plane currents. *J. Fluid Mech.* **258**, 77–104.

HACKER, J., LINDEN, P. F. & DALZIEL, S. B. 1996 Mixing in lock-release gravity currents. *Dyn. Atmos. Oceans* **24** (1), 183–195.

HALLWORTH, M. A., HUPPERT, H. E., PHILLIPS, J. C. & SPARKS, R. S. J. 1996 Entrainment into two-dimensional and axisymmetric turbulent gravity currents. *J. Fluid Mech.* **308**, 289–311.

HARRIS, T. C., HOGG, A. J. & HUPPERT, H. E. 2001 A mathematical framework for the analysis of particle-driven gravity currents. *Proc. R. Soc.* A **457**, 1241–1272.

HOGG, A. J. 2006 Lock-release gravity currents and dam-break flows. *J. Fluid Mech.* **569**, 61–87.

HOGG, A. J., HALLWORTH, M. A. & HUPPERT, H. E. 2005 On gravity currents driven by constant fluxes of saline and particle-laden fluid in the presence of a uniform flow. *J. Fluid Mech.* **539**, 349–385.

HOGG, A. J. & PRITCHARD, D. 2004 The effects of hydraulic resistance on dam-break and other shallow inertial flows. *J. Fluid Mech.* **501**, 179–212.

HOGG, A. J., UNGARISH, M & HUPPERT, H. E. 2000 Particle-driven gravity currents: asymptotic and box-model solutions. *Eur. J. Mech.* (B/ *Fluids)* **338**, 139–165.

HOGG, A. J. & WOODS, A. W. 2001 The transition from inertia to bottom-drag-dominated motion of turbulent gravity currents. *J. Fluid Mech.* **449**, 201–224.

HOULT, D. P. 1972 Oil spreading on the sea. *Annu. Rev. Fluid Mech.* **4**, 341–368.

HUPPERT, H. E. 1982 The propagation of two-dimensional and axisymmetric viscous gravity currents over a rigid horizontal surface. *J. Fluid Mech.* **121**, 43–58.

HUPPERT, H. E. & SIMPSON, J. E. 1980 The slumping of gravity currents. *J. Fluid Mech.* **99**, 785–799.

KURGANOV, A. & TADMOR, E. 2000 New high-resolution central schemes for nonlinear conservation laws and convection–diffusion equations. *J. Comput. Phys.* **160**, 241–282.

LEVEQUE, R. J. 2002 *Finite Volume Methods for Hyperbolic Problems*. Cambridge University Press.

MARINO, B. M., THOMAS, L. P. & LINDEN, P. F. 2005 The front condition for gravity currents. *J. Fluid Mech.* **536**, 49–78.

MATHUNJWA, J. S. & HOGG, A. J. 2006 Stability of gravity currents generated by finite volume releases. *J. Fluid Mech.* **562**, 261–278.

MORTON, B. R., TAYLOR, G. & TURNER, J. S. 1956 Turbulent gravitational convection from maintained and instantaneous sources. *Proc. R. Soc.* A **234** (1196), 1–23.

PARKER, G., FUKUSHIMA, Y. & PANTIN, H. M. 1986 Self-accelerating turbidity currents. *J. Fluid Mech.* **171**, 145–181.

PARKER, G., GARCIA, M., FUKUSHIMA, Y. & YU, W. 1987 Experiments on turbidity currents over an erodible bed. *J. Hydraul. Res.* **25** (1), 123–147.

ROSS, A. N., DALZIEL, S. B. & LINDEN, P. F. 2006 Axisymmetric gravity currents on a cone. *J. Fluid Mech.* **565**, 227–254.

ROTTMAN, J. W. & SIMPSON, J. E. 1983 Gravity currents produced by instantaneous releases of a heavy fluid in a rectangular channel. *J. Fluid Mech.* **135**, 95–110.

SHERMAN, F. S., IMBERGER, J. & CORCOS, G. M. 1978 Turbulence and mixing in stably stratified waters. *Annu. Rev. Fluid Mech.* **10**, 267–288.

SHIN, J. O., DALZIEL, S. B. & LINDEN, P. F. 2004 Gravity currents produced by lock exchange. *J. Fluid Mech.* **521**, 1–34.

SIMPSON, J. E. 1999 *Gravity Currents in the Environment and the Laboratory*. Cambridge University Press.

SIMPSON, J. E. & BRITTER, R. E. 1979 The dynamics of the head of a gravity current advancing over a horizontal surface. *J. Fluid Mech.* **94**, 477–495.

SORGARD, E. 1991 A numerical, three-layered, stationary salt wedge model. *J. Geophys. Res* **96**, 12739–12754.

STOKER, J. J. 1957 *Water Waves: The Mathematical Theory with Applications*. Interscience.

TICKLE, G. A. 1996 A model of the motion and dilution of a heavy gas cloud released on a uniform slope in calm conditions. *J. Hazard. Mater.* **49** (1), 29–47.

TORO, E. F. 2009 *Riemann Solvers and Numerical Methods for Fluid Dynamics: A Practical Introduction*. Springer.

TURNER, J. S. 1973 *Buoyancy Effects in Fluids*. Cambridge University Press.

TURNER, J. S. 1986 Turbulent entrainment: the development of the entrainment assumption, and its application to geophysical flows. *J. Fluid Mech.* **173**, 431–471.

UNGARISH, M. 2009 *An Introduction to Gravity Currents and Intrusions*. Chapman and Hall/CRC.